



# Reinforcement learning based adaptive power pinch analysis for energy management of stand-alone hybrid energy storage systems considering uncertainty<sup>☆</sup>

Bassey Etim Nyong-Bassey<sup>a, \*</sup>, Damian Giaouris<sup>a</sup>, Charalampos Patsios<sup>a</sup>,  
Simira Papadopoulos<sup>b, c</sup>, Athanasios I. Papadopoulos<sup>b</sup>, Sara Walker<sup>a</sup>, Spyros Voutetakis<sup>b</sup>,  
Panos Seferlis<sup>d</sup>, Shady Gadoue<sup>e</sup>

<sup>a</sup> School of Engineering, Newcastle University, Newcastle NE1 7RU, United Kingdom

<sup>b</sup> Chemical Process and Energy Resources Institute, Centre for Research and Technology Hellas, 57001, Thessaloniki, Greece

<sup>c</sup> Department of Automation Engineering ATEL, Thessaloniki, Greece

<sup>d</sup> Department of Mechanical Engineering, Aristotle University of Thessaloniki, 54124, Thessaloniki, Greece

<sup>e</sup> Aston University, School of Engineering and Applied Science, Birmingham, United Kingdom

## ARTICLE INFO

### Article history:

Received 8 April 2019

Received in revised form

23 August 2019

Accepted 23 November 2019

Available online 2 December 2019

### Keywords:

Hybrid energy storage systems

Energy management strategies

Model predictive control

Kalman filter

Reinforcement learning

## ABSTRACT

Hybrid energy storage systems (HESS) involve synergies between multiple energy storage technologies with complementary operating features aimed at enhancing the reliability of intermittent renewable energy sources (RES). Nevertheless, coordinating HESS through optimized energy management strategies (EMS) introduces complexity. The latter has been previously addressed by the authors through a systems-level graphical EMS via Power Pinch Analysis (PoPA). Although of proven efficiency, accounting for uncertainty with PoPA has been an issue, due to the assumption of a perfect day ahead (DA) generation and load profiles forecast. This paper proposes three adaptive PoPA-based EMS, aimed at negating load demand and RES stochastic variability. Each method has its own merits such as; reduced computational complexity and improved accuracy depending on the probability density function of uncertainty. The first and simplest adaptive scheme is based on a receding horizon model predictive control framework. The second employs a Kalman filter, whereas the third is based on a machine learning algorithm. The three methods are assessed on a real isolated HESS microgrid built in Greece. In validating the proposed methods against the DA PoPA, the proposed methods all performed better with regards to violation of the energy storage operating constraints and plummeting carbon emission footprint.

© 2019 Elsevier Ltd. All rights reserved.

## 1. Introduction

Growing concerns over the impact of greenhouse gas emission on the environment has led to policy initiatives to advance the proliferation of renewable energy sources (RES) (such as wind turbines and solar panels), for distributed generation (DG). Furthermore, in remote areas without access to an electrical grid,

RES are a favourable electrification alternative when compared to the cost of deploying high-voltage transmission lines and associated power losses [1–3]. The use of RES (particularly in a stand-alone microgrid (MG)) can reduce the reliance on backup diesel generators (DSL) which have a high carbon emission impact on the environment [4,5]. Nevertheless, due to weather stochasticity, some RES can have predictable but variable power output and so, incorporating energy storage technology with RES can mitigate this variability. Multiple energy storage technologies (e.g. battery and hydrogen) with complementary properties (such as life cycle, seasonality, power and energy density etc.) are often combined to further mitigate the RES variability. This is the concept of hybrid energy storage systems (HESS) as shown in Fig. 1 [6,7]. This system was designed and built in Xanthi, Greece in collaboration with

<sup>☆</sup> The short version of this paper was presented at ISCAS2018, May 27–30, Florence, Italy. This paper is a substantial extension of the ISCAS2018 Conference paper.

\* Corresponding author. School of Engineering, Newcastle University, Newcastle NE1 7RU, United Kingdom.

E-mail address: [B.E.Nyong-Bassey1@ncl.ac.uk](mailto:B.E.Nyong-Bassey1@ncl.ac.uk) (B.E. Nyong-Bassey).

CERTH and SUNLIGHT [8] and it is been used here as a case study. The mathematical model of each asset has been previously validated [9] by the authors and real load/weather profiles have been used.

In such systems, when supply exceeds demand and a local battery is completely charged, the energy from the RES can, for example, be converted to hydrogen ( $H_2$ ) by an electrolyser (EL) for long term storage (as opposed to the battery that can be seen as short-term storage option). Then, the hydrogen can be used when demand exceeds supply, by means of a fuel cell (FC) [7,10]. The HESS thereby can reduce the dumped load in times of excess supply, and further reduce the need for backup DSL in times of excess demand [11]. Newer innovative hydrogen production approach, which relies on internal rather than external reforming of fuel mixtures into mass production of electric and thermal energy carriers, with high efficiency, based on the use of Solid Oxide Fuel Cells (SOFCs) have recently been investigated. In Ref. [12], an intermediate temperature solid oxide electrolyser stack is fed with carbon dioxide ( $CO_2$ )-steam mixture at the anode. Here the fuel mixture is reformed into  $CO - H_2$  mixture while at the cathode, oxygen fed into the system is converted into ions. The oxygen ions generate current by moving through the electrolyte towards the anode to combine with the  $CO - H_2$  mixture to produce  $CO_2$  and water. Furthermore, authors [13] investigated the use of low weight as well as low cost high temperature steam electrolysis (HSTE) stack for durability and performance to highlight current density and steam conversion ratio at the temperature of  $800^\circ C$ . In Ref. [14] the anion exchange membrane (AEM) FC which is attractive due to its outstanding fast electrochemical kinetics, low dependence on non-precious catalyst and water removal mechanisms was presented. In Ref. [15] an analytic model for alkaline anion exchange membrane FC is proposed. The authors in their investigation, illustrated more anode humidification improved performance. Nevertheless, a systems-level analysis approach has been implemented in this work, hence, the impact on the HESS as a result of integrating these newer  $H_2$  technological innovations which were highlighted will be an

interesting subject for future investigation.

Despite the advantages offered by a HESS, the heterogeneity of the components/devices introduces complexity due to the need to account for different forms/characteristics of energy flows between multiple assets and for numerous decision parameters in energy management strategies (EMSs) used for HESS control. To address such complexity, several studies have proposed the use of if-then-else rules, artificial intelligence (AI) (such as fuzzy logic controllers, neural networks, and genetic algorithms), linear and dynamic programming and advanced control techniques to realise EMSs for HESS [16–18]. Development of EMSs using if-then-else rules in the form of hierarchical diagrams is widely used in published literature due to its computational efficiency [16].

In Ref. [19] a rule-based EMS was proposed for domestic microgrid. The rules are such that the load requirement at each time interval is compared with the PV power and which only fulfils the load power requirement, and whenever the output power of the PV is greater and given the battery level, any excess is either used for charging operation or arbitrage or to cover the deficit. The rule based EMS had accurate result and faster processing time in comparison with an optimisation based EMS. However, this approach is largely heuristic and limited to very few potential options, omitting numerous alternatives which may improve the HESS performance, as illustrated in Ref. [7]. In addition, fuzzy logic controller which is classically rule-based has enhanced adaptation and robustness in contrast to a conventional rule base controller as depicted in the case of energy management (EM) of islanded MG in Ref. [20].

In Ref. [21] self-organising and dynamic fuzzy logic decision making was used to improve electric vehicle (EV) efficiency by estimating the required output power of a FC based on the driving load requirement and state of charge of a BAT in MATLAB environment. In Ref. [22], the merits underling the integration of hybrid energy systems, specifically; a FC, BAT and supercapacitor in an EV are first analysed. Thereafter, an active power flow control technique is proposed based on optimal control theory with the

Nomenclature		$\Delta k$	Time interval
$AEEND$	Available excess energy for the next day	$\delta$	The proportion of flow $j$
$BAT$	Battery	$\eta_{CV}, \eta_{PV}, \eta_{FC}, \eta_{EL}$	DC converter, PV panel, fuel cell, electrolyser efficiency factors
$C_l$	The capacity of accumulator $l$	$\varepsilon_i(k)$	Binary variable for the state of the $i$ th dispatchable unit
$DSL$	Diesel generator	$\rho_i^t$	The binary variable related to the temporal conditions of the accumulator
$EL$	Electrolyser	<i>Subscripts/superscripts</i>	
$FC$	Fuel Cell	$SOAcc$	Accumulator or energy storage
$HT$	Hydrogen Tank	$Avl$	Availability of resources
$G$	A fixed reward	$Gen$	Override logic for PoPA energy dispatchable units $FC$ and $EL$
$\mathcal{I}$	Identity matrix $\in \mathbb{R}^{n \times n}$	$Req$	Demand for resources
$LD$	Load	$k$	Time step
$MAE$	Minimum absorbed energy	$i$	Index of Converter
$MOES$	Minimum outsourced energy supply	$l$	Accumulator
$s^-$	Previous state before a transition by the agent	$max$	maximum
$SOAcc_l^t$	State of accumulator $l$	$min$	minimum
$S_{lp}^t$	Lower pinch limit or utility	$m, n$	Model and the plant respectively
$S_{up}^t$	Upper pinch limit or utility	$i_c$	A set of controllable energy converter elements for PoPA targeting
$POW$	Power flow	$\rightarrow$	The arrow head indicates the direction of flow of energy/material from source to sink
$PGCC$	Power grand composite curve		
$\mathcal{R}$	Zero mean Gaussian noise $\in \mathbb{R}^{n \times n}$		
$\mathcal{U}$	Input $\in \mathbb{R}^{m \times 1}$		
$W1, W2$	Penalty weights which control the propagation of the negative reward exerted on the agent		
$WT$	Water tank		



### 1.1. Applications of PoPA for electric power systems sizing and design

Several researchers have considered PoPA for electric power systems sizing and design. In Refs. [41,46] the grand composite curve was realised by integrating the energy demand and supply over time, and then it was used to optimally size an isolated power generation system. Additionally, in Ref. [47] the PoPA was utilised as a combination of both the graphical analysis and numerical approach with the aid of the power cascade analysis and storage cascade table for optimal sizing of the hybrid power system. The extended Power Pinch analysis (EPoPA) in Ref. [48] was proposed as an enhancement to the PoPA in order to optimally design renewable energy systems integrated with battery-hydrogen assets as well as a DSL. These studies on PoPA for sizing MG assets with the exclusion of [46] in which chance constrained programming was used to achieve technical and economic feasibility, were realised without recourse to uncertainty.

### 1.2. Applications of PoPA for energy management

Apart from the use of PoPA in electric power systems sizing and design, it has also been used, by the authors, as an EM tool, as first reported in Refs. [5,7,49]. More specifically, in Ref. [7] the power grand composite curve (PGCC) was realised within a model predictive control (MPC) framework for the first time with a day ahead (DA) forecast to infer and effect (EM) decisions in a HESS standalone MG. By shaping the PGCC, a series of optimal control decisions for the activation and duration of the HESS operation were determined. The effectiveness of this approach was limited by the assumption of a perfect DA weather and load forecast.

### 1.3. Generic approaches to uncertainty

The pinch analysis despite being a well-established process integration recovery and conservation technique for assets such as waste management, water, heat, and carbon emission requires consideration and expansion in power systems application [42]. Also, as highlighted, most literature on PoPA have not dealt with uncertainty, as these studies have mostly relied on the assumption of perfect (or ideal) weather forecast and load profile with the exception of [46] where uncertainty was considered in the sizing of a MG asset. Consequently, the significant impact of uncertainty, imposes the need to integrate PoPA tools with a complementary technique, especially when consistency is so desired. The techniques which account for uncertainty in EM can fundamentally be classed as either predictive or reactive approach [50]. These predictive or reactive approaches may perhaps be considered in PoPA application, whereby, the scheduling of dispatchable units are realised with or without prior consideration for the impact of an impending uncertainty respectively. The reactive approach uses the latest state feedback for re-computation, upon model mismatch due to uncertainty, which may be expensive when seeking an optimum solution in the event of frequent perturbation. The predictive technique may employ stochastic programming, fuzzy programming, robust optimisation, machine learning techniques, in order to infer the optimal control action that negates the effect of uncertainty [51–53]. Furthermore, the linear Kalman filter, first presented by Kalman in 1960 for solving the Wiener problem has since been applied extensively in areas of control system, short-term prediction, navigation tracking and for systems state estimation associated with uncertainty [54]. In Ref. [55] the ensemble Kalman filter was combined with a multiple regression model to enhance forecasting accuracy of electricity load. Similarly, in Ref. [56] the Kalman filter was used recursively to estimate short-

term hourly load demand forecast parameters based on the historical load and weather data and the current measurements of the time-varying parameters. Moving away from the well-known prediction methods, the work of [57] on temporal difference (TD) learning, a model-free reinforcement learning (RL) algorithm, introduced a prediction method which relies on the experience of successive predictions to infer the behaviour of an unknown system. This was a paradigm shift to the conventional approach which depended only on the difference between the actual and predicted outcome. Hence, RL is a machine learning technique, suitable for solving a Markov decision process (MDP) which involves sequential optimal decision making under uncertainty. Thus, many researchers have sought to deploy several machine learning algorithms in an MDP. In Ref. [58], machine learning algorithms such as policy iteration and value iteration Dynamic programming, and RL techniques such as the least squares policy iteration, Q-Learning, and SARSA were reviewed for MDPs. Specifically of interest, is the Q-learning, a class of model-free RL, a similar algorithm to Sutton's (1988) TD learning [56], first introduced by Watkins in 1989, which proffers an intelligent agent with the learning ability to act optimally in a MDP based on experience [59]. In Q-learning, an agent seeks to maximise the sum of expected reward by acting optimally with respect to any given circumstance (referred to as a state). Typically, an agent will evaluate a state, and will then undertake an action either in an exploitative or exploratory manner thereafter and finally will receive an instant reward, while transitioning to a new state. Q-learning has tremendous success in robotics, especially in mobile robot navigation and obstacle avoidance [60,61]. In Ref. [62] the Dyna AI architecture was proposed to integrate both learning, and experience, based on online planning, as well as reactive execution in a stochastic environment.

Furthermore, in Ref. [63] a comparative study of MPC and Monte Carlo RL on a non-linear deterministic system with known uncertainty dynamics was undertaken. More recently [64], harnessed the merits of the MPC and RL control strategies to form an adaptive controller for a heat pump thermostat based on the suggestion of [63]. The adaptive controller maximised energy savings while tracking a varying temperature set-point for thermal comfort, more effectively than the MPC or RL alone.

The application of RL based energy management for HESS has mostly been considered in literature with respect to hybrid Electric vehicle while only a few have considered microgrid systems. In Ref. [65] energy management based on a 2 steps-ahead RL framework was proposed for a grid connected microgrid which comprised consumers load, ES, wind turbine. The RL is formulated as a multi-criteria decision making tool, aided by a 2 steps-ahead prediction of available wind power via a Markov chain model. This approach allowed the learning agent to optimally utilise the WT, independently of the grid to charge the ES, while maximising the use of the ES during peak demands. Hence, enabling an intelligent consumer to learn a stochastic scenarios while incorporating experience based optimal actions. In Ref. [66] deep RL EMS which uses a convolution neural net to extract relevant time series information, from a large continuous non-handcrafted feature space is proposed to address stochastic electricity production in a residential MG. In Ref. [67] the authors propose an EMS which applies a decentralised cooperative multi-agents enabled Fuzzy Q-learning to a standalone MG. The formulation of the continuous input states entails the use of five membership functions and the action space comprising a fuzzy set pertaining to each MG asset and rules base in conjunction with a reward formulation, shapes the agent's continuous action policy. In Ref. [68] the authors proposed a real-time EM algorithm to optimise performance and energy efficiency with power split control for a hybrid (battery and ultra-capacitor) tracked vehicle for various road driving conditions. A



speedy Q-Learning algorithm is used to accelerate the convergence of a multiple transition probability matrix which is also updated whenever the error norm exceeds a set criteria. In our work we have excluded the use of a Markov chain to model a stochastic transition probability matrix (TPM) of the MDP, as this not mandatory in the development a RL framework [69]. Though in Refs. [68,70] Markov chain is used to model a stochastic TPM which is updated periodically when a specific criterion is exceeded by the magnitude of an induced matrix norm and kull-back divergence respectively. This is in contrast to an earlier proposed method in Ref. [71] where the authors for the first time applied reinforcement learning technique (specifically TD( $\lambda$ )) to minimise the fuel consumption of a hybrid electric vehicle without the need for prior knowledge or stochastic information of the driving cycle, and uses only a partial hybrid electric vehicle model. Nevertheless, our proposed RL formulation requires only the (corrected) adaptive Pinch analysis target, strictly for evaluating the environment state and scalar reward which the dyna-Q learning agent receives after taking an action in a given state. Furthermore, the step wise non-linear optimisation used to derive the optimal control strategy in Refs. [68,70] and a backward-looking optimisation in Ref. [71] is replaced with a heuristic graphical based adaptive power pinch analysis MPC framework, which we have proposed in our work. Thus, eliminating the computational cost associated with building a TPM offline, as well as solving a complex non-convex optimisation EMS for HESS (particularly with heterogeneous energy and flow mix as in our case, where we have to deal with the intrinsic interaction of power, hydrogen, and water flow between sub-systems). Furthermore, we have omitted detailed operational considerations with regards to losses associated with device level operation, since the considered EM approach is at the systems level.

Nevertheless, evaluation and formulation of the scalar reward in aforementioned RL papers excluding [70] which applies a backward-looking optimisation, have mostly been implemented subjectively and without recourse to a systematic approach which determines the ideal optimal action strategy as in the use of a corrected adaptive PoPA. Hence, these rewards are based on a local maximisation which increases the operational cost and incurred excess energy losses in contrast with a global maximum insight which the corrected adaptive PoPA offers.

#### 1.4. Main contributions and novelties

It is clear that PoPA has rarely addressed the issue of uncertainty and only in a case of HESS sizing, while the PoPA approach has significant advantages (described above) in cases of adaptive EM. To this end, such advantages have been previously exploited by the authors within an MPC framework, however under limiting assumptions of perfect weather and load forecasting. The focus of this work is therefore on addressing the issue of RES/load forecast error which is bound to occur in a realistic scenario, in the context of the PoPA approach.

Three novel adaptive PoPA schemes are proposed based on an EMS algorithm for an islanded HESS aimed at significantly reducing the effect of forecast error while shaping the PGCC. It has to be noted here that the islanded HESS that is being used here as a case study, has been designed and built by the authors at CERTH in collaboration with SUNLIGHT [8], and the mathematical models of the assets have been previously experimentally validated [9].

More specifically, the main contributions of this work are as follows:

I. The DA PoPA in Ref. [49] for EM of HESS has been adapted for the first time, to realise an 'Adaptive PoPA' [72], by re-shaping the PGCC in a multi-step, look ahead, receding horizon MPC framework as shown in Fig. 2. This method offers a simple but effective means

to counter the effects of forecast error.

II. A Kalman filter for the first time, has been used in conjunction with the aforementioned Adaptive PoPA [72], to predict the State of Charge of the battery ( $SOAcc_{BAT}^m$ ) based on the likelihood estimation of uncertainty. The algorithm is more sophisticated than the Adaptive PoPA but nevertheless computationally efficient and offers a preventive measure as an improvement. Furthermore, the occurrence of the forecast error is not dependent on the corrective action, as in case (I), which may improve the algorithmic performance.

III. A RL-based adaptive PoPA (RL + Adaptive) method has been proposed for the first time, in the context of the dyna Q-learning algorithm. The dyna Q-learning algorithm entails learning a policy by means of rewarding an agent based on the next state of the system after inferring a control action given the current state of the system. Thus, the agent learns an EMS by solving for the optimal action policy. Additionally, with the action policy, the agent decides the de/activation of the dispatchable units in accordance with a corrected PGCC shaped with the Adaptive PoPA. This approach does not assume that the underlying uncertainty is normally distributed in the procedure that minimises the mean squared error in the estimated state-of-charge, as in case (II). This may improve the algorithmic performance, hence it is worth investigating.

The three approaches are analysed in this paper. Furthermore, a sensitivity analysis with hydrogen uncertainty is used to evaluate the proposed methods against the DA PoPA. The rest of the paper is structured as follows: Section 2 briefly describes the Power Pinch concept. Section 3 presents the formalisation of the receding adaptive MPC-PoPA concept. In section 4 and 5, the proposed Kalman filter state estimator approach with Adaptive PoPA and the RL Adaptive PoPA algorithms are presented, respectively. The results are presented in Section 6, and Section 7 provides a conclusion.

## 2. Power pinch analysis for energy management of hybrid energy storage systems

### 2.1. Generic description

In order to understand how Pinch Analysis can be used to determine an EMS in a HESS (as shown in Fig. 1), infer a generic islanded energy system with multiple energy carriers (like electrical and hydrogen), multiple storage assets (like a BAT and a HT), generation assets (like photovoltaic panels (PV)), controllable assets that can transform an energy from one carrier to another (like a FC and an EL) and a load (possibly for each energy carrier). Also, for each storage component we set up operating limits that should not be violated, say  $S_{LO}$  and  $S_{UP}$  which is the minimum and maximum allowed stored energy/material respectively.

The first step to apply the PoPA concept is to define the Power Grand Composite Curve (PGCC) for each energy carrier, which is the integration of all uncontrolled energy demands and generation in the system for that carrier for each instance. When the system is at a specific instant  $k$ , we predict the PGCC as shown in Figure 2a by assuming that the controllable assets are not activated and we check if the predicted PGCC violates any of the aforementioned limits. The predictive horizon is based on an hourly interval which spans for 24 h  $\in [k : N]$ , where  $k$  is the  $i^{th}$  hour in a day and  $N$  indicates the end of the day (or 24th h). The hourly interval  $\Delta k$  is expressed as the difference between two successive time steps;  $\Delta k = [(k+1) - k]$  where,  $k$  and  $k+1$  are the current and next time step respectively. The interval between the current time step  $k$  and the end of the horizon  $N$  is given as  $(N - k)/\Delta k$ , and the entire horizon would have 23 intervals, if  $k$  is the first hour, 01 : 00h and  $N = (k+23)$  is the 24 : 00h of the day. If the PGCC violates a limit at a specific instant, then at an appropriate instant before the violation

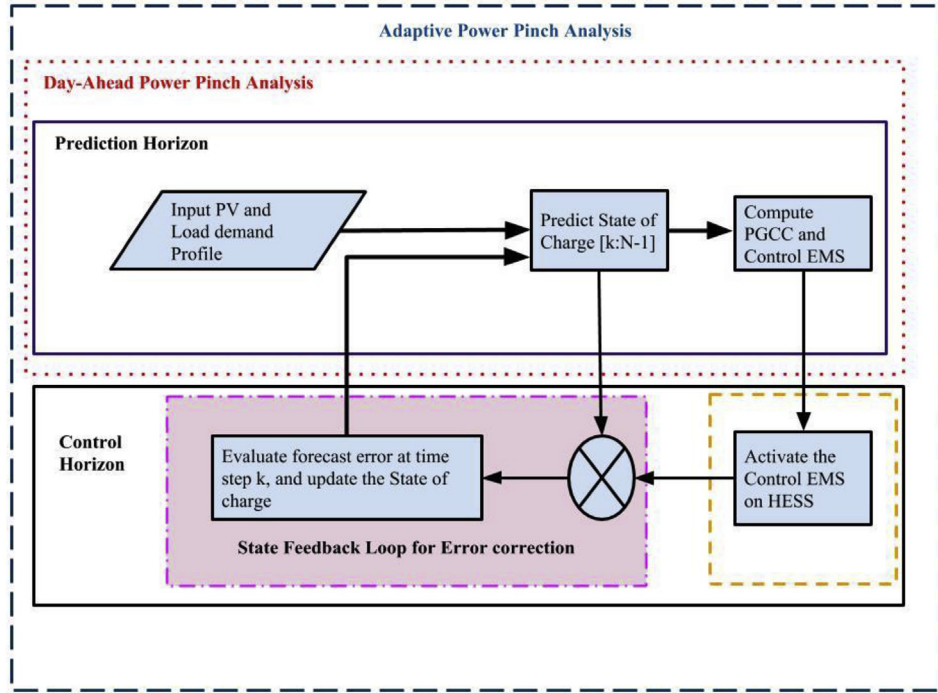


Fig. 2. Schematics of the adaptive power pinch analysis EMS for HESS [40].

occurs, a suitable controlled asset will be activated in a control horizon of interval  $24 \text{ h} \in [k : N]$  with equivalent time duration as in the predictive horizon in order to provide/remove the necessary energy/material so that the system limits are not exceeded. In order to better describe the aforementioned concepts, a specific motivating case will be presented in the next subsection.

## 2.2. Motivating case

In the HESS as shown in Fig. 1, let the stored electrical energy (i.e. state of charge,  $SOAcc$ ) be the quantity that we wish to control within specific operating limits. Therefore, an EMS is derived in prediction horizon using a DA strategy and implemented on the HESS in a control horizon. In the prediction horizon,  $SOAcc$  is plotted (dotted black line in Fig. 3a) at an hourly time step  $k$ , for a daily (24 h) span as defined in section 2.1. The PoPA enables the identification of deficit and excess energy targets, which must be successively met, in order to prevent the  $SOAcc$  in the control horizon from falling below the lower pinch utility (or limit)  $S_{Lo}$  (say 30%) and/or rising above the upper pinch utility  $S_{Up}$  (say 90%).

At first, the control strategy aims to determine the deficit energy target at the minimum  $SOAcc$ , denoted as  $S_{min}$ . In this case study, the deficit results from the absence of sufficient energy supply by the PV. The deficit energy target is then the amount of energy needed to ensure  $SOAcc$  avoids the violation of the  $S_{Lo}$  limit at time  $k + k_{min}$ . The PGCC determines the minimum amount of out-sourced electricity supply (MOES) required in order to violate  $S_{Lo}$ . A dispatchable asset, (such as a FC) indicated by a red arrow pointing upward at time  $k$  shown in Fig. 3b, supplies the energy needed to shift the PGCC above  $S_{Lo}$ .

Secondly, the control strategy aims to determine the excess energy target at the maximum  $SOAcc$ , denoted as  $S_{Max}$ . The excess energy target is then the amount of energy that needs to be dumped in order to avoid the violation of the  $S_{Up}$  limit at time  $k + k_{max}$ . This is denoted as the minimum excess energy for storage (MEES). Thus, the MEES is recovered for storage by a dispatchable

asset (such as an electrolyser (EL)) denoted by the red arrow pointing downwards shown in Fig. 3b.

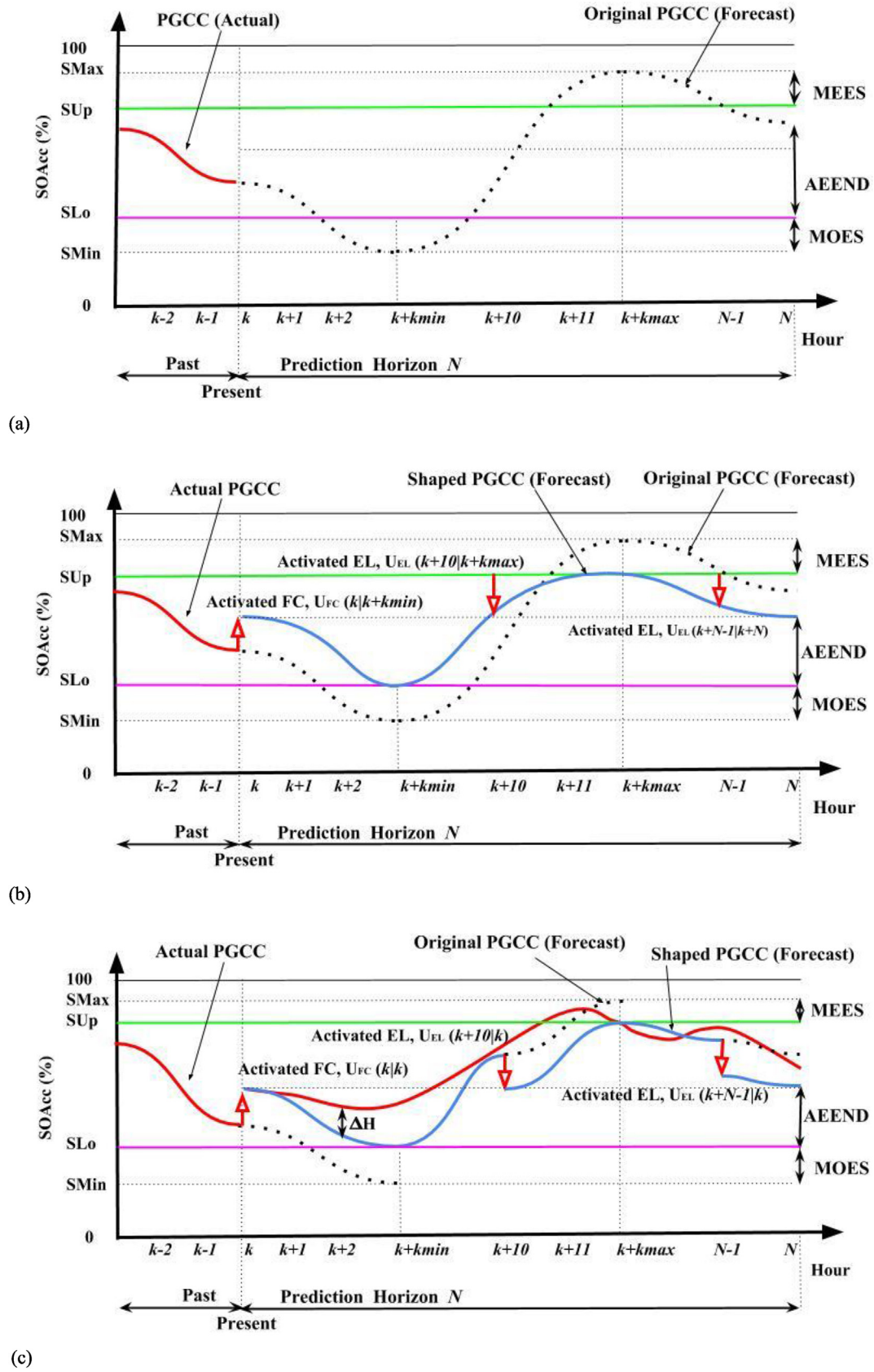
Thirdly, to preserve the duty cycle of the energy storage, the available energy for the next day (AEEND) i.e.  $SOAcc$  at time step  $N$  has to be matched to the  $SOAcc$  at time step  $k$ , by activating dispatchable assets (either the FC or EL) at time step  $N - 1$ .

Consequently, by shifting the entire PGCC up or down (black dot-dashed line in Fig. 3b), there are instances where the PGCC reaches (but no longer exceeds) the  $S_{Lo}$  or  $S_{Up}$  at times  $k + k_{min}$  and  $k + k_{max}$ , which is termed the Pinch point. Therefore, the shifted PGCC which resolves the PoPA EMS is responsible for the instant and duration for which the energy targeting resources are activated/deactivated in the control horizon [5,7,49,73].

However, effectively realising the optimal PoPA EMS via DA operation requires an accurate load and weather forecast model for an ideal PGCC plot, which is impractical due to uncertainty for most real applications. The effect of uncertainty,  $\Delta H$  due to RES variability and stochasticity of electricity demand, causes a mismatch between the actual (red line) and predicted (blue line)  $SOAcc$  as illustrated in Fig. 3c and consequent violation of  $S_{Up}$  and the duty cycle constraint. Therefore, the utilisation of a feedback loop is crucial to improve the excess energy recovery and reliability indices. It can also reduce the need for (potentially higher carbon emission) energy imports to the system.

## 3. Adaptive power pinch analysis

The effects of uncertainty on renewable energy sources and electricity demand with respect to the DA-PoPA operation have been highlighted in section 2. Thus, in this section we adapt the DA-PoPA, to create an Adaptive PoPA which uses a receding horizon MPC approach. In a prediction horizon spanning 24 h with hourly interval  $\Delta k$  and time step  $k$ , as defined in section 2, the dispatchable control variable  $U_c(k)$  is determined based on the PoPA targets. Accordingly,  $U_c(k)$  determined in the prediction horizon is activated in control horizon at each time interval  $k$ . Furthermore,



the  $SOAcc$  as a function of the minimum energy recovery is achieved with regards to the Adaptive PoPA expressed as follows:

$$J_{Pinch} = \min_{U_c} \sum_{k=1}^{N-1} f(\varepsilon_i(k), SOAcc_l^m(k), U_c(k)) \quad (1)$$

Subject to the Power Pinch analysis constraints:

$$S_{Lo}^l \leq SOAcc_l^m(k) \leq S_{Up}^l \quad (2)$$

$$SOAcc_l^n(k_1) \equiv SOAcc_l^m(N) \quad (3)$$

$$\varepsilon_{EL}(k) + \varepsilon_{FC}(k) \leq 1 \quad (4)$$

where,  $k_1$  is the first hour,  $\varepsilon_i(t)$  is a binary variable for the dispatchable asset's state  $i \in \{FC, EL\}$ , (see appendix I),  $U_c(k)$  represents the PoPA EMS control variable and subscript  $c \in \{FC, EL\}$  indicates the dispatchable asset. In  $SOAcc_l^{m,n}$  the superscripts  $m$  and  $n$  refers to the predicted and real  $SOAcc$  respectively, and subscript  $l \in \{BAT, HT, WT\}$  indicates the energy storage of note.

The constraints imposed by (2) ensures the pinch operating limits are not violated. The duty cycle of the energy storage is preserved by the terminal constraint (3) to infer the available energy at the end of the prediction horizon  $N$  (AEEND). The binary variable constraint (4) prevents the simultaneous dispatch of assets that concurrently consume and produce the same energy carrier (e.g. FC and EL).

The following explanation is for one asset, the BAT, but is relevant to all asset types. At every time step  $k$ , the proposed algorithm compares the forecast and real  $SOAcc_{BAT}^n(k)$  for inconsistency or forecast deviation via a state feedback close loop [72]. As illustrated in Fig. 4a,  $\Delta H$  exceeds 5% at time  $k+2$ . Therefore, state correction is effected at the next time  $k+kmin$ , to decrease the forecast deviation between the predicted  $SOAcc_{BAT}^m$  and actual  $SOAcc_{BAT}^n$ . The re-computation of the PGCC (dotted black line in Fig. 4a) which follows reveals an anticipated violation of the  $S_{UP}$  such that  $SOAcc_{BAT}^m$  is a maximum at time  $k+11$ , and the AEEND. Thus, the predicted PGCC is re-shaped as shown in Fig. 4b (blue line) with the EL dispatched at time  $k+10$  and  $N-1$ .

The error  $e(k)$  and magnitude of uncertainty  $\Delta H$  between the forecast and real state of charge of the Battery are expressed in (5) and (6) respectively as follows:

$$e(k) = SOAcc_{BAT}^n(k) - SOAcc_{BAT}^m(k|k-1) \quad (5)$$

$$\Delta H(k) = |e(k)| \quad (6)$$

where,  $SOAcc_{BAT}^m(k|k-1)$  is the predicted battery state of charge at time  $k$  based on a prior time step  $k-1$  and  $SOAcc_{BAT}^n(k)$  is the actual battery state of charge at time step  $k$ .

Furthermore, if  $\Delta H$  is greater than the deviation threshold  $\xi$  at any sampling instance, the PoPA is repeated in the predictive horizon in order to determine the optimal dispatch and schedule sequence from that instant up until time  $N$ .  $\xi$  (which may be varied or decreased for a tighter bound) is set at 5%, to ensure minimal forecast deviations as well as to reduce any computational cost. Re-computation of the PGCC uses equations (7) and (8) as follows:

$$SOAcc_{BAT}^m(k) := \begin{cases} f(\Delta H(k)) & \text{if } \Delta H(k) > \xi \\ SOAcc_{BAT}^m(k|k-1) & \text{Otherwise} \end{cases}, \forall k \quad (7)$$

where,  $f(\Delta H(k))$  corrects  $SOAcc_{BAT}^m$  as follows:

$$f(\Delta H(k)) = \begin{cases} SOAcc_{BAT}^m(k|k-1) + \Delta H(k) & e(k) > 0 \\ SOAcc_{BAT}^m(k|k-1) - \Delta H(k) & e(k) < 0 \end{cases} \quad (8)$$

#### 4. Kalman filter adaptive power pinch analysis

In the previous section a reactive error correction strategy has been presented, the adaptive PoPA, which does not consider the effect of future un-modelled uncertainty. This may result in a limit violation as shown in Fig. 5a. Therefore, the Kalman filter is incorporated into the Adaptive PoPA framework for robustness, as the battery's future state ( $SOAcc_{BAT}^m(k+1|k)$ ) is predicted while incorporating the effect of uncertainty at each time interval upon the availability of the most recent battery state ( $SOAcc_{BAT}^n(k)$ ) measurement. In order to predict the battery's state, a priori error covariance  $\mathcal{P}_{k-1}$  matrix with respect to  $SOAcc_l$ , updates the Kalman gain  $K_{G(k)}$  as follows:

$$K_{G(k)} = \mathcal{P}_{k-1} \mathcal{J}^T [\mathcal{J} \mathcal{P}_{k-1} \mathcal{J}^T + \mathcal{R}_k]^{-1} \quad (9)$$

The updated Kalman gain is used to update the a priori covariance matrix:

$$\mathcal{P}_k = [\mathcal{J} - K_{G(k)} \mathcal{J}] \mathcal{P}_{k-1} \quad (10)$$

The most recent output state measurement  $SOAcc_l^n(k)$  is used to update the estimated state as follows:

$$SOAcc_l^m(k) = SOAcc_l^m(k|k-1) + K_{G(k)} (SOAcc_l^n(k) - \mathcal{J}_k SOAcc_l^m(k|k-1)) \quad (11)$$

The posterior error covariance matrix is also updated:

$$\mathcal{P}_{k+1} = A \mathcal{P}_k A^T + \mathcal{R}_k \quad (12)$$

where,  $A \in l \times l$  is an identity state transition matrix for the energy storages  $l$ ,  $\mathcal{J}_k \in l \times l$  is an identity matrix and  $\mathcal{R}_k$  is the covariance noise matrix related to the uncertainty in  $SOAcc_l^m$ .

Therefore, this formulation can be used to consider a multi-vector case of uncertainty in the energy storages. Nevertheless, in this work only the  $SOAcc$  of the BAT is the parameter directly impacted by the LD and RES uncertainty since it acts as the central integrating ES, and a change in the  $SOAcc$  of HT and WT can be considered deterministic as well as contingent on the controlled activation of FC or EL. Therefore, the variance and co-variance of  $SOAcc$  of HT and WT in  $\mathcal{P}_k$  matrix are set to 0. Furthermore, the  $SOAcc_{BAT}^m(k) \in [SOAcc_l^m(k)]$  is determined in (11) in order to identify the uncertainty over successive  $k$ - steps ahead and consequently to compute the PGCC. Thereafter, the PGCC is re-shaped via PoPA minimum energy targeting as before. Thus, a sequence of dynamic EMSs which satisfies both the PoPA  $S_{Lo}$  and  $S_{Up}$  constraints with uncertainty projection is realised in the prediction horizon for the optimal dispatch and scheduling of energy resources in the control horizon. The concept is illustrated in Fig. 5b, where the cyan plot indicates the PGCC re-shaped via the Kalman + Adaptive PoPA. The violation of the  $S_{Up}$  at time  $k+11$ , which occurred with the Adaptive PoPA EMS in Fig. 5a, is avoided by dispatching the EL to recover correct MESS at time  $k+10$ . Likewise, the procedure is repeated for the AEEND constraint. Fig. 6, shows the Kalman + Adaptive PoPA algorithm.



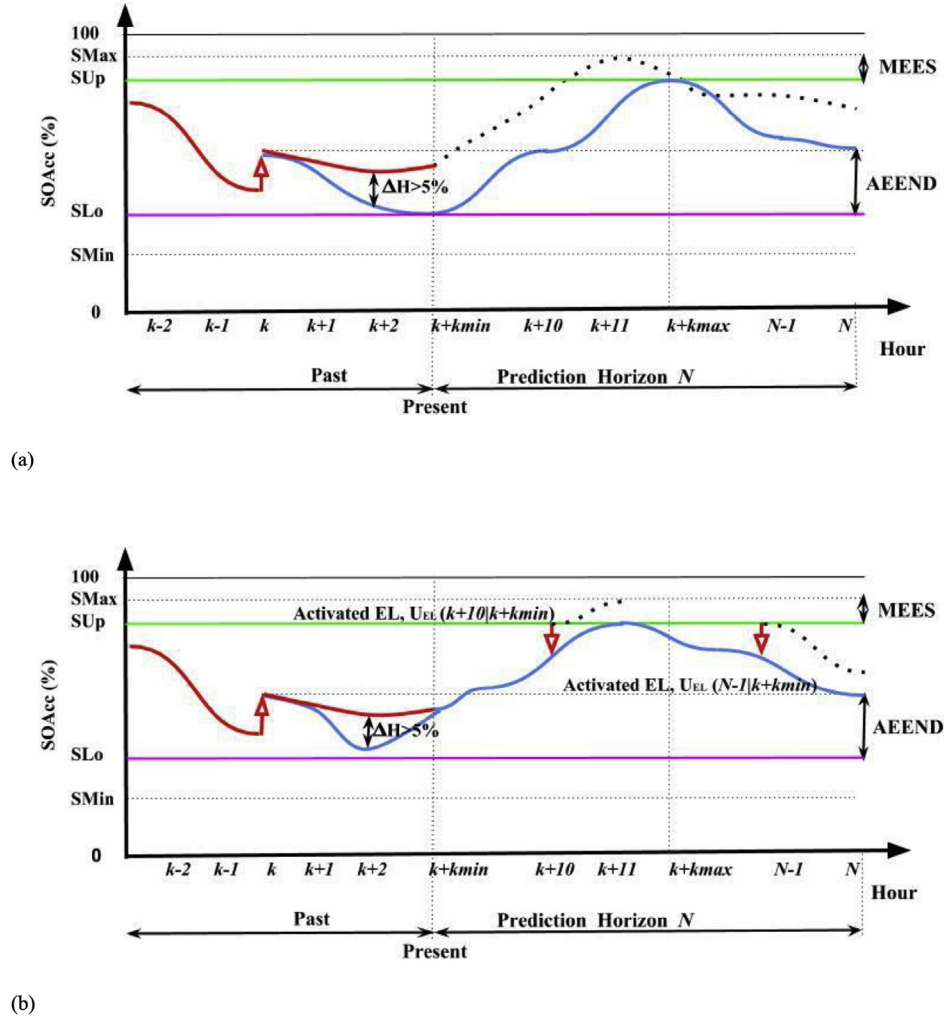


Fig. 4. (a) State error correction and (b) re-shaped PGCC with Adaptive PoPA.

## 5. Reinforcement Learning Adaptive Power Pinch analysis

The approach presented in this work involves formulating the uncertainty problem as a MDP considered in the discrete time step  $k$ , where an agent has to act optimally by inferring an action in each state as determined by the adaptive MPC PoPA trajectory.

The MDP is a tuple  $(S, A, R, S', A')$  where:

$\mathcal{S}$ : is a set of discrete  $n$ -states  $\mathcal{S} = \{s_1, s_2, \dots, s_n\}$  and  $s_k$  denotes the state of the environment at time step  $k$ .

In this work,

$$s_k := f(\text{SOAcc}_{\text{BAT}}^m(k), \text{SOAcc}_{\text{BAT}}^n(k), e(k)) \quad (13)$$

$\mathcal{A}$ : is a discrete set of  $n$ -actions for selection by the agent  $\mathcal{A} = \{a_1, a_2, \dots, a_7\}$  and  $a_k$  indicates the selected action at time  $k$ .

Furthermore, the set of dispatchable assets for the PGCC shaping is expressed as follows:

$U_c(t) \subseteq \mathcal{A}_k := \{a_1, \delta_1 \text{FC}, \delta_2 \text{FC}, \delta_3 \text{FC}, \delta_4 \text{EL}, \delta_5 \text{EL}, \delta_6 \text{EL}\}$  Where,  $\delta_x$ ,  $x \in [1 : 6]$ , represents percentage proportions  $\{10, 50, 90\}$  and  $\{10, 50, 100\}$  of corresponding flow of energy/material  $F_{\text{FC} \rightarrow \text{BAT}}^{\text{Pow}}(k)$  and  $F_{\text{BAT} \rightarrow \text{EL}}^{\text{Pow}}(k)$  respectively to a selected action and  $a_1$  denotes null action.

$\mathcal{T}(s, a, s')$ : is the probability of transitioning to a next state  $s'$  from state  $s$  over a given set of transitions when an action  $a$  is chosen.

$\mathcal{S} \times \mathcal{A} \rightarrow R$ : An immediate reward  $r_t$  is received as a result of the system state transition  $\mathcal{T}(s, a)$  to the next state  $s'$  by mapping state and action pair  $(s, a)$  due to a decision making policy  $\pi$ .

Therefore, both the transition and reward probability distributions are implicitly Markov properties where the future state  $s'$  only depends on the present state  $s$ . The current action  $a$  is independent of the past state(s)  $s^-$  that lead to the present state [74,75].

$$\mathcal{T}(s'|s^-, s, a) = \mathcal{T}(s'|s, a) \quad (14)$$

The model of the system is required for initial training of the agent in order to infer the control action on the actual system from the MPC-PoPA. The agent adapts to the real system over time and retrain on newer samples. The MDP learning agent learns the optimal policy  $\pi^*(a|s)$  from accumulated past experience which maps an optimal action to a given state. Hence, this maximises the cumulative scalar reward return as shown in (15).

$$\mathcal{V}^\pi = E \left[ \sum_{k=1}^{\infty} \gamma^{k-1} r_k(s_1, a_1 | \pi) \right] \quad (15)$$

The Q-function  $Q^\pi(s, a)$  for a given MDP represents the optimal value function  $\mathcal{V}^\pi$ .

The agent learns the optimal action to take in the environment through experience by taking actions in the environment while

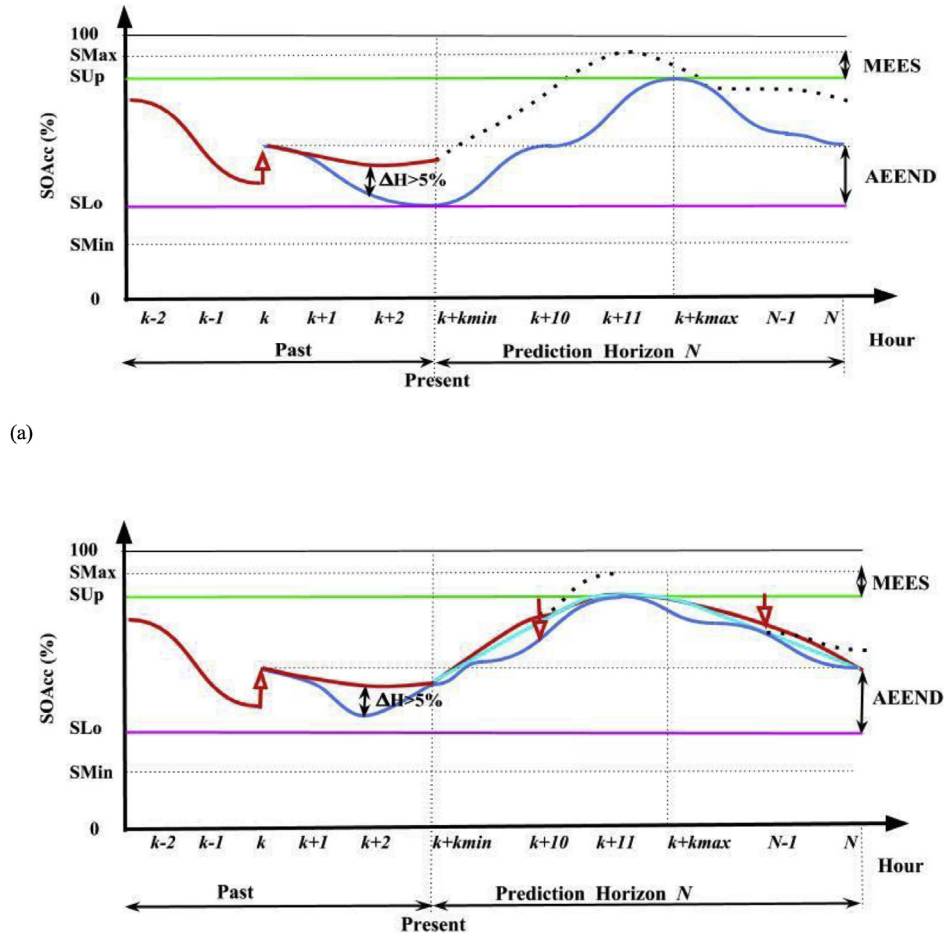


Fig. 5. (a) PGCC shaped with Adaptive PoPA and (b) PGCC shaped with Kalman + Adaptive PoPA.

learning the optimal policy.

The Q-learning rule after taking an action  $a$  in a state  $s$ , obtaining a reward  $r$  and transitioning to  $s'$  is as follows:

reinforce the learning agent's Q - value to guarantee optimality. The model-free learning happens using the Q-learning algorithm and switches to a Monte Carlo algorithm at  $N - 1$  which denotes the

$$Q_k(s, a) = \begin{cases} Q_k(s, a) + \alpha [r_k + \gamma \max_{a'} Q_{k+1}(s', a') - Q_k(s, a)] & \forall k = [1, 2, \dots, N-2] \\ Q_k(s, a) + \alpha [r_k - Q_k(s, a)] & \forall k = N-1 \\ Q_k(s, a) & \forall k = N \end{cases} \quad \alpha, \gamma \in \left[ 0, < 1 \right] \quad (16)$$

where  $\alpha, \gamma$  are learning rate and future reward discount factor with the future discounted reward omitted during the update of the agent at a terminal state at time step  $N - 1$ .

### 5.1. Planning stage for the Q-learning agent

The MPC-PoPA model is used to bootstrap the Q-learning agent to ensure that the agent acts optimally with respect to tracking the PoPA trajectory, computed offline prior to online deployment so as to minimise and avoid exploiting costly mistakes on the real system. The advantage of the Q-algorithm is that the agent garners experience from the real environment and retrain offline by replaying the experience after each episode at time  $N$  to further

terminal state (horizon) for the agent, as shown in (16). Therefore, the learning involves two steps; a direct and indirect learning, from the model and from the actual system (environment) respectively.

### 5.2. Action selection

The action selection approach in (17) which has been modified to include safety precautions in critical states (near the Pinch limits), is based on the probability  $(1 - \theta)$  of selecting a *greedy* policy  $\pi(s)$  over a random action with probability of  $\theta$  [76,77]. This approach exploits the best action as indicated by the maximum value function  $Q^{\pi^*}(s, a)$  for a given state while performing exploration with the inverse probability  $(\theta)$  of acting greedily. This strategy strikes a balance between exploration and exploitation

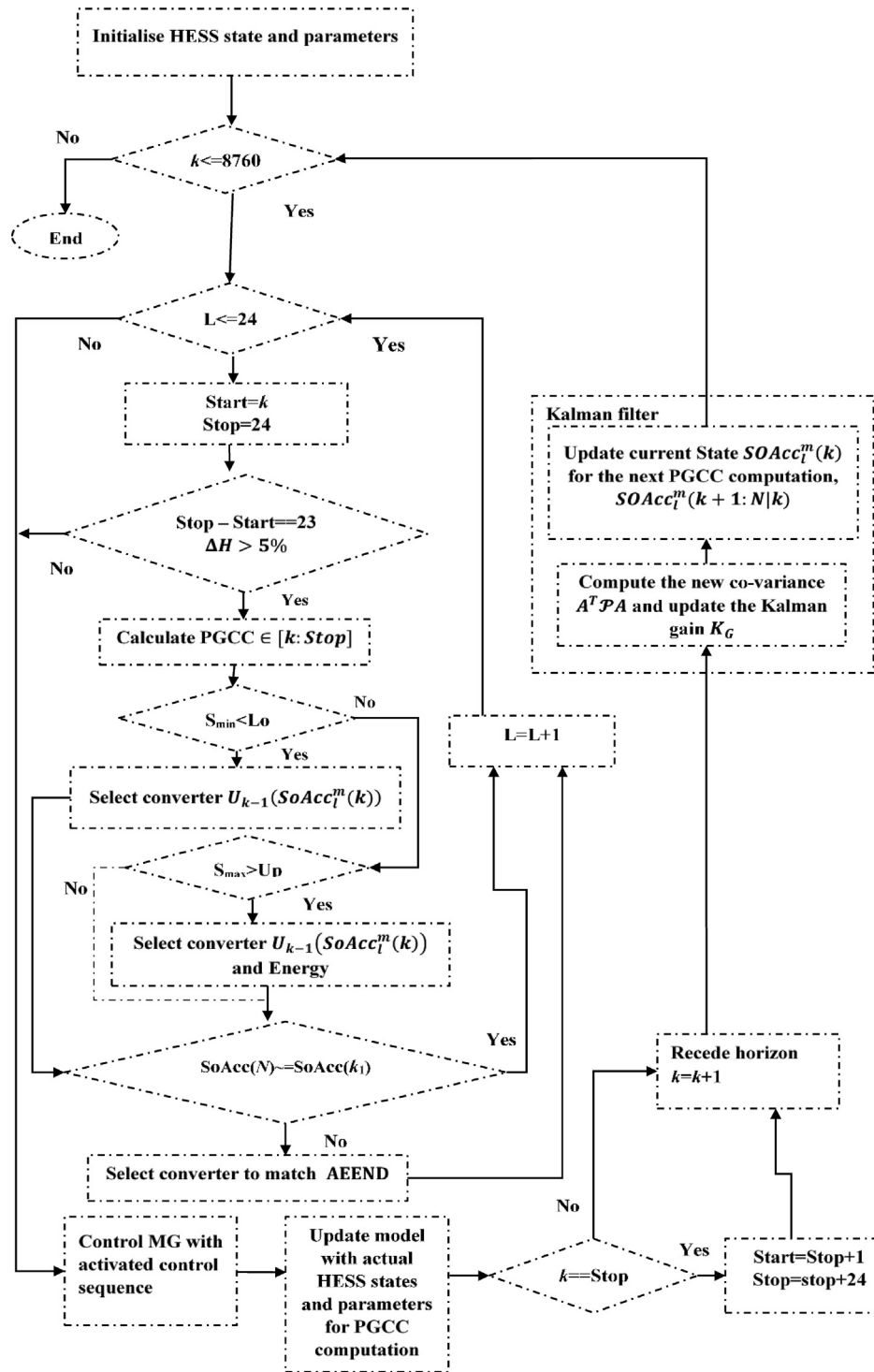


Fig. 6. Kalman + Adaptive power pinch algorithm.

while satisfying the famous Bellman's principle of optimality [78], minimising the deviation of the system controlled by the learning agent from the Pinch target, and exploring the state space. If the  $SOAcc_{BAT}^n(k)$  is less than  $Lo$  or greater than  $Up$ , the FC and EL are dispatched by the agent respectively. Furthermore, the AEEND constraint imposed at the end of the day is achieved by overriding the agent's action with the Adaptive PoPA's EMS. The action policy  $\pi(s)$  is expressed as follows:

$$\pi(s) = \left\{ \begin{array}{ll} a_k(s) & \text{If } U < \text{greedy action probability } (1 - \theta) \\ \delta_3 FC & \text{if } U > \text{greedy action probability } (1 - \theta) \wedge \\ \delta_6 FC & \text{if } U > \text{greedy action probability } (1 - \theta) \wedge SOAcc_{BAT}^n(k) \leq 30\% \\ \text{select a random action} & \text{Otherwise} \end{array} \right\} \quad (17)$$

where.

$U$  is a randomly generated value between 0 and 1 given each  $k$  time step.

representing a squared error penalty cost function and constant penalty factor respectively.

The magnitude of the  $W_1$  penalty factor is such that it increases proportionally to the absolute squared error deviation from the pinch target at that instant and the systems state if the agent takes a suboptimal action as shown in equation (22). Furthermore, the rewarded function in (23)–(25) is able to update the agent  $Q(s, a)$  regardless of whether the availability proposition  $\varepsilon_i^{Avl}(k)$  (see ap-

pendix II) for both the FC and EL assets are met, while exploiting an action which minimises the error cost.

A typical illustration; if the operating point dictated by Adaptive

$$a_k(s) := \left\{ \begin{array}{ll} \delta_3 FC & SOAcc_{BAT}^n(k) \leq 30\% \\ \delta_6 EL & SOAcc_{BAT}^n(k) \geq 90\% \\ \argmax_{a_k(s) \in \{a_1, \delta_n FC\}, n \in [1:3]} Q(s_k, a_k) & SOAcc_{BAT}^n(k) \geq 30\% \wedge SOAcc_{BAT}^n(k) \leq 40\% \\ \argmax_{a_k(s) \in \{a_1, \delta_n EL\}, n \in [4:6]} Q(s_k, a_k) & SOAcc_{BAT}^n(k) \geq 80\% \wedge SOAcc_{BAT}^n(k) \leq 90\% \\ \argmax_{a_k(s) \in A_t} Q(s_k, a_k) & \text{otherwise} \end{array} \right\} \quad (18)$$

### 5.3. Reward function formalisation

In order to train the Q-learning agent, a suitable reward function is expressed mathematically. This is such that the agent follows the optimal policy  $\pi^*(s)$  which minimises the cost function between the agent's off-policy and the adaptive MPC PoPA trajectory, and is expressed as follows:

$$J_\pi(SOAcc_{BAT}^n) = \lim_{k \rightarrow N-2} E \left[ \sum_{k=1}^{N-2} \left| SOAcc_{BAT}^m - SOAcc_{BAT}^n \right|^2 + (\gamma J_\pi(s_{k+1})) \right] \quad (19)$$

Thus, it follows that:

$$\min_{U, J_\pi(SOAcc_{BAT}^n)} \triangleq \lim_{k \rightarrow \infty} \argmax_{a_k \in A_k} E \left[ \sum_{k=N-2}^{\infty} \left( \gamma^{k-1} \mathcal{R}(s_{k+1}, a_{k+1}) \right)^{-1} \right] \quad (20)$$

The reward function in (21) is aimed at accelerating learning. It comprises of a fixed reward  $G$ , with penalty factors  $W_1$  and  $W_2$ ,

PoPA anticipates future energy deficit and requests activation of the FC, while the agent activates the EL, a penalty would suffice. Thus, the penalty function, serves as a closed loop negative feedback to the agent. Therefore, in order to obtain the maximum reward  $G$  at a given time step, the action performed by the agent, must satisfy the consequent conditional proposition. As shown in (23)  $U_{cmin}$  is contingent on function D and E in equations (24) and (25) respectively. Where, functions D and E are performed abstractly by iterating over all actions  $a_i$  the agent can perform. Specifically, assuming the  $SOAcc_{BAT}^m(k+1)$  is less than 80%, function D is used and thus by iterating over all actions  $a_i \in [1 : 7]$ ,  $U_{cmin}$  becomes the minimum (infimum) action which results in  $SOAcc_{BAT}^m(k+1)$  being greater or equal to  $SOAcc_{BAT}^n(k+1)$ . This suppresses the excessive usage of the FC. Similarly, where function E suffices, the maximum (supremum) action which results in  $SOAcc_{BAT}^m(k+1)$  being less than or equal to  $SOAcc_{BAT}^n(k+1)$  becomes  $U_{cmin}$  such that the EL is used optimally.

Furthermore, if the action performed by the agent is not equal ( $\neg$ ) to  $U_{cmin}$ , and consequently  $SOAcc_{BAT}^m(k+1)$  becomes less than or equal to  $SOAcc_{BAT}^n(k+1)$  a negative penalty denoted by  $-W_1$  ensues in order to apprise the agent from exploiting adverse actions which over discharges the BAT.

Also, where the agent performs  $a_k$  not equal to  $U_{cmin}$ , but which results in the  $SOAcc_{BAT}^n(k+1)$  becoming greater than or equal to  $SOAcc_{BAT}^m(k+1)$ , a penalty  $W_1$  is deducted from the maximum



$$\mathcal{R}(s_k, a_k) = \left\{ \begin{array}{l} G \\ -W_1 \\ G - W_1 \\ -(W_1 + W_2) \end{array} \right\} \left\{ \begin{array}{l} \left[ \begin{array}{l} SOAcc_{BAT}^n(k+1) \geq SOAcc_{BAT}^m(k+1) \wedge a_k \neq U_{cmin} \wedge \\ [SOAcc_{BAT}^n(k+1) > S_{Lo}^l \wedge SOAcc_{BAT}^n(k+1) < S_{Up}^l] \end{array} \right] \\ \left[ \begin{array}{l} [SOAcc_{BAT}^n(k+1) \leq SOAcc_{BAT}^m(k+1)] \wedge a_k \neq U_{cmin} \wedge \\ [SOAcc_{BAT}^n(k+1) > S_{Lo}^l \wedge SOAcc_{BAT}^n(k+1) < S_{Up}^l] \end{array} \right] \\ \left[ \begin{array}{l} [SOAcc_{BAT}^n(k+1) \geq SOAcc_{BAT}^m(k+1)] \wedge a_k \neq U_{cmin} \wedge \\ [SOAcc_{BAT}^n(k+1) > S_{Lo}^l \wedge SOAcc_{BAT}^n(k+1) < S_{Up}^l] \end{array} \right] \\ \left[ \begin{array}{l} [SOAcc_{BAT}^n(k) \leq SOAcc_{BAT}^n(k+1)] \wedge \\ [SOAcc_{BAT}^n(k) \geq S_{Up}^l \wedge SOAcc_{BAT}^n(k+1) \geq S_{Up}^l] \wedge \\ [a_k \neq U_{cmin} \vee SOAcc_{BAT}^n(k+1) \geq S_{Up}^l \wedge a_k \neq U_{cmin}] \end{array} \right] \\ \left[ \begin{array}{l} [SOAcc_{BAT}^n(k) \leq SOAcc_{BAT}^n(k+1)] \wedge \\ [SOAcc_{BAT}^n(k) \geq S_{Up}^l \wedge SOAcc_{BAT}^n(k+1) \geq S_{Up}^l] \wedge \\ [a_k \neq U_{cmin} \vee SOAcc_{BAT}^n(k+1) \leq S_{Lo}^l \wedge a_k \neq U_{cmin}] \end{array} \right] \end{array} \right\} \vee \quad (21)$$

reward  $G$  in order to dampen excessive usage of the FC. Similarly, a penalty  $-(W_1 + W_2)$  is used to accelerate the agent's learning curve if successive violations of any of the pinch limits occur as a result of suboptimal action.

The reward function proposition for  $\mathcal{S} \times \mathcal{A} : \mathcal{R}(\mathcal{S}, \mathcal{A})$  is implemented as follows;

$$U_{cmin} : \left\{ \begin{array}{ll} D & SOAcc_{BAT}^m(k+1) > S_{Lo}^l \wedge SOAcc_{BAT}^m(k+1) \leq (S_{Up}^l - 10\%) \\ E & SOAcc_{BAT}^m(k+1) > (S_{Lo}^l + 50\%) \wedge SOAcc_{BAT}^m(k+1) < (S_{Up}^l) \end{array} \right\} \quad (23)$$

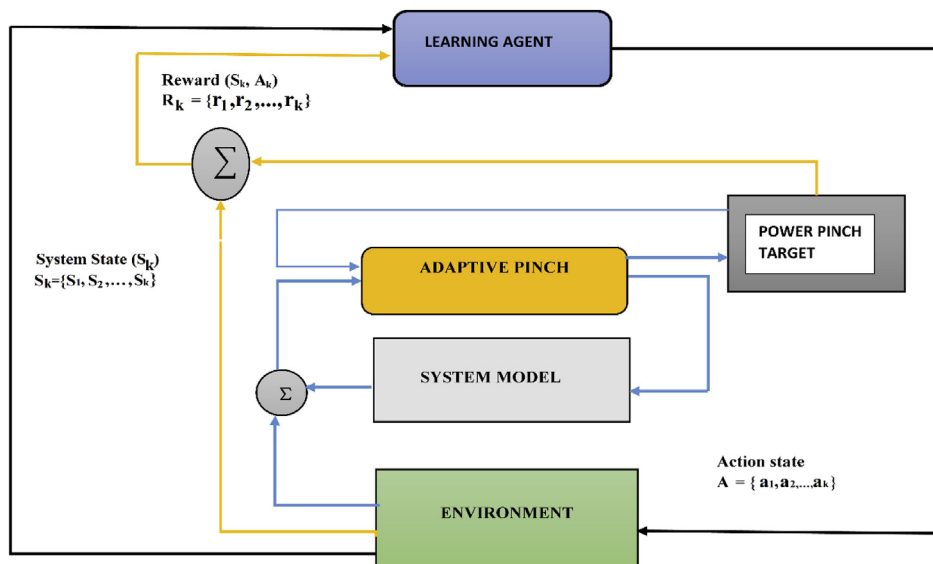


Fig. 7. Reinforcement Learning Adaptive Power Pinch architecture.

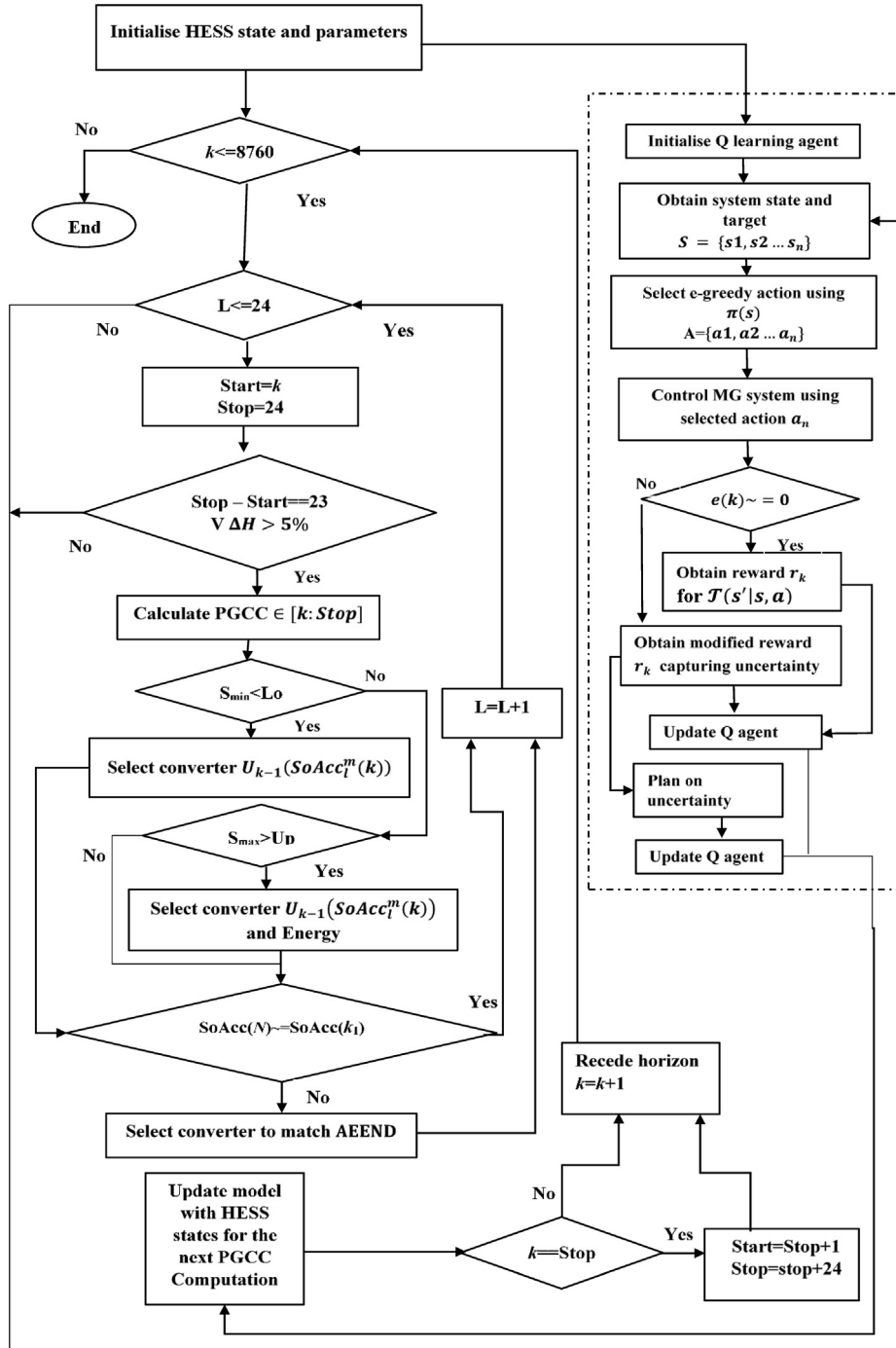


Fig. 8. RL + adaptive power pinch algorithm.

**Table 1**  
HESS Micro-grid parameters [9].

System Components	Specification
Load (peak)	2200 W
PV (66.64 W rated power)	217
DSL	2210 W
BAT	3000 Ah/48 V
FC	3000 W
EL	4000 W
HT	30 bar, 15 m <sup>3</sup>
$\eta_{CV}, \eta_{PV}, \eta_{FC}, \eta_{EL}$	0.95, 0.10, 0.87, 0.87

where,  $W_1$  and  $W_2$  are penalty factors for reward shaping.

$$W_1 = [(SOAcc_l^m(k+1) - SOAcc_{BAT}^m(k+1)) / SOAcc_{BAT}^m(k+1)]^2 \quad (22)$$

The action which results in the minimum optimal control action is derived abstractly as follows:

where,

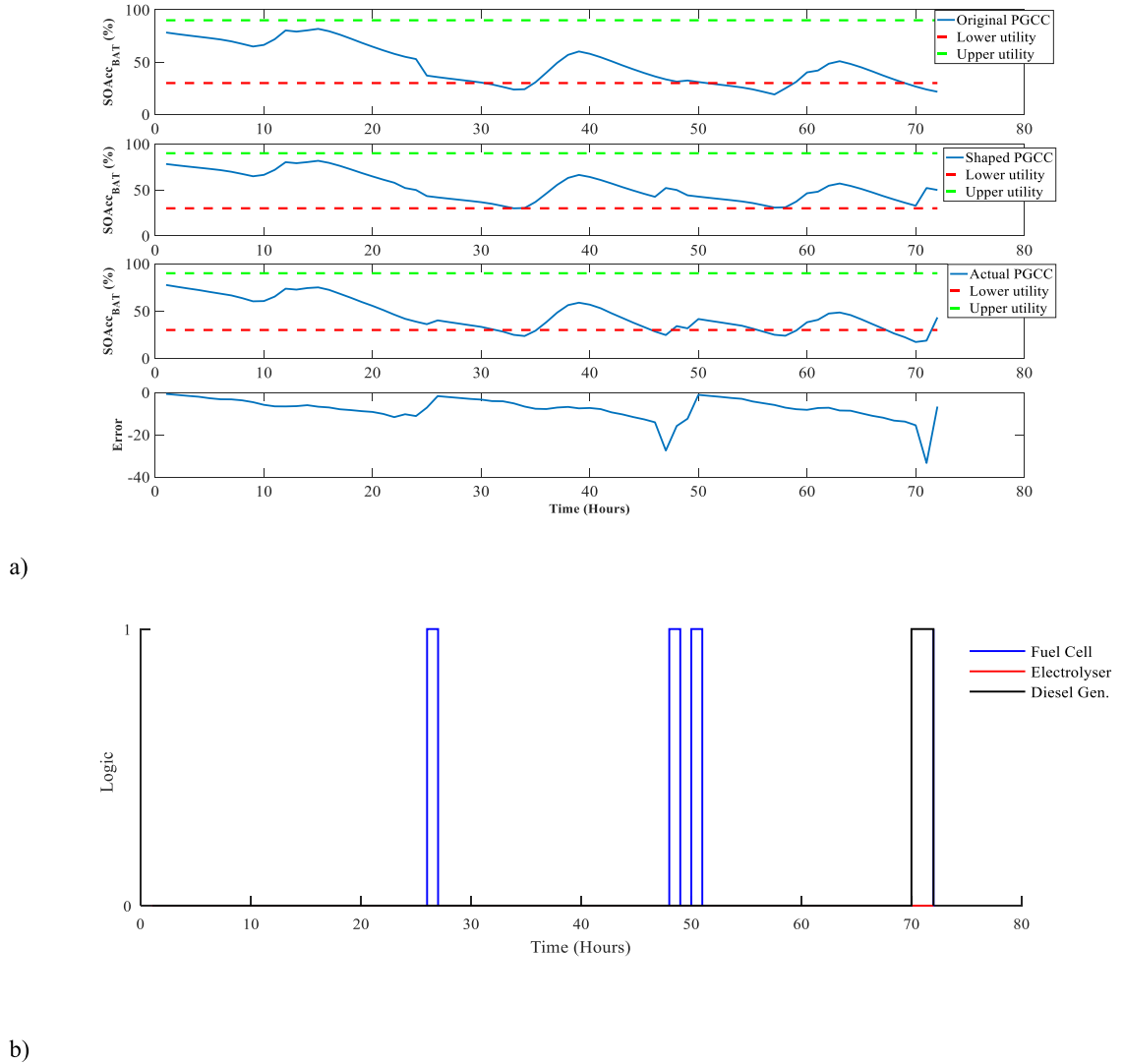


Fig. 9. a) DA-PoPA response and b) Dispatchable Logic state for the first 72 h of the year.

$$D := \inf \left\{ \left( \left( SOAcc_{BAT}^m(k+1) \right) \left| \sum_{i=1}^7 Q(a_i, s_{k+1}) \right. \right) \times \right\} \geq SOAcc_{BAT}^n(k+1) \quad (24)$$

$$E := \sup \left\{ \left( SOAcc_{BAT}^m(k+1) \right) \left| \sum_{i=1}^7 Q(a_i, s_{k+1}) \right. \right\} \leq SOAcc_{BAT}^n(k+1) \quad (25)$$

During the online deployment, the PoPA target is modified respectively with the MOES or MEES so as to capture the effect of uncertainty after  $S_{LO}$  and  $S_{UP}$  violation occurs at any instant as follows:

$$SOAcc_{BAT}^m(k|k) := \begin{cases} S_{UP}^l & SOAcc_{BAT}^n(k) > S_{UP}^l \\ S_{LO}^l & SOAcc_{BAT}^n(k) < S_{LO}^l \end{cases}, \forall t \text{ if } \exists \Delta H(k) \neq 0 \quad (26)$$

The reward function is modified to incorporate the MOES or

MEES thus guaranteeing the model-free agent will act optimally in the event of uncertainty to maximise the expected reward:

$$J_{Pinch}(SOAcc_{BAT}^n) + J_e(\Delta H) = \min_{U_c} J_{\pi}(SOAcc_{BAT}^n) \quad (27)$$

Furthermore, by performing the optimal policy  $\pi^*$  the corresponding cost is as follows:

$$J_{\pi}^*(SOAcc_{BAT}^n) \rightarrow \lim_{k \rightarrow \infty} E \left[ \sum_k \gamma \left( J_{Pinch}(SOAcc_{BAT}^n) + J_e(\Delta H) \right) \right] \quad (28)$$

Since the cost of the error due to uncertainty tends to zero when following the optimal policy,  $J_{\pi}^*(s)$ , the agent incorporates the uncertainty estimation into the PoPA:

$$\lim_{k \rightarrow \infty} J_{\pi(k)}^*(SOAcc_{BAT}^n) \leq \gamma J_{Pinch(k)}(SOAcc_{BAT}^n) \quad (29)$$

The expected cost following the pinch analysis and uncertainty propagation is less than following only the PoPA model. Hence, the experience of the agent integrated into the MPC Adaptive PoPA

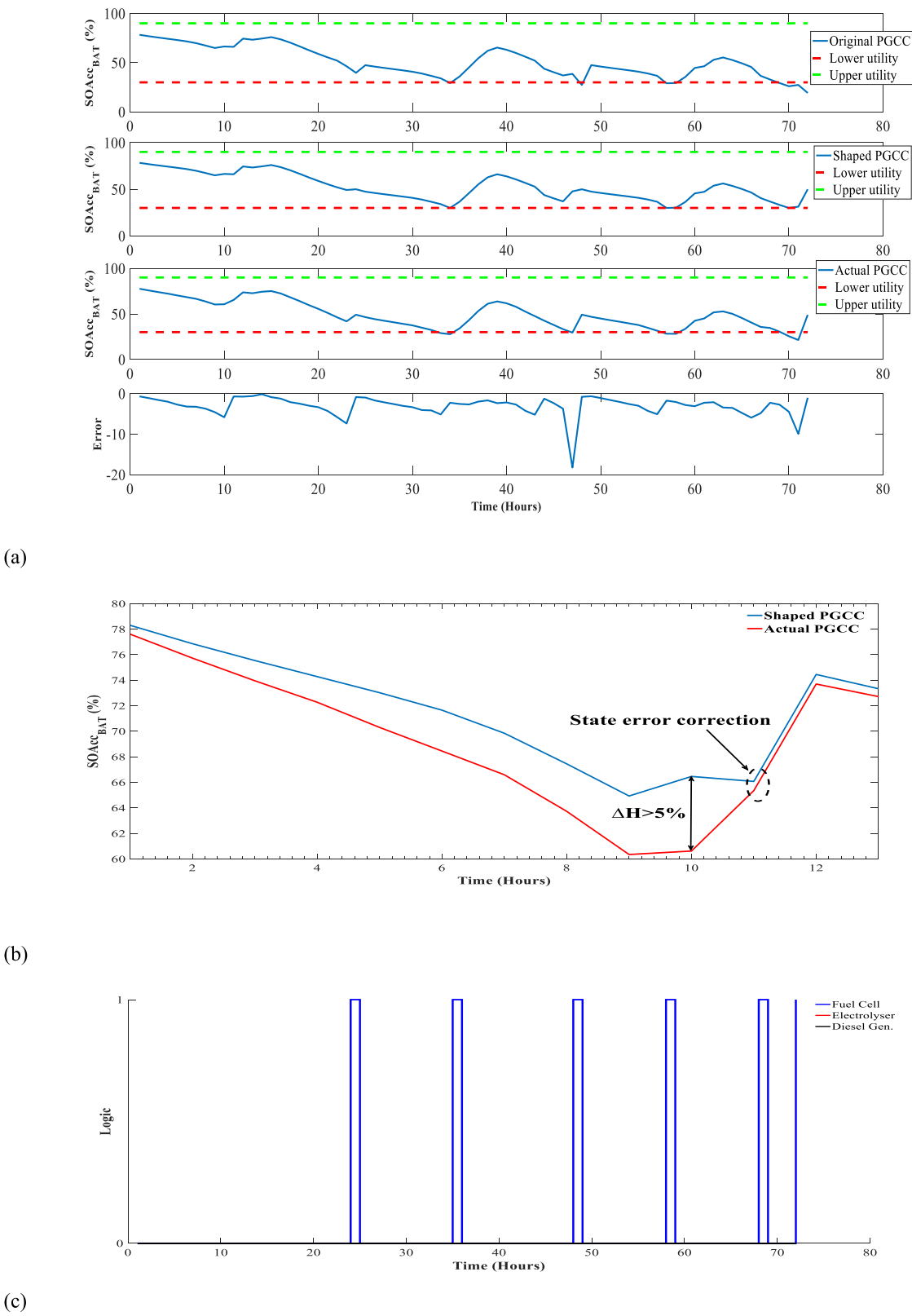
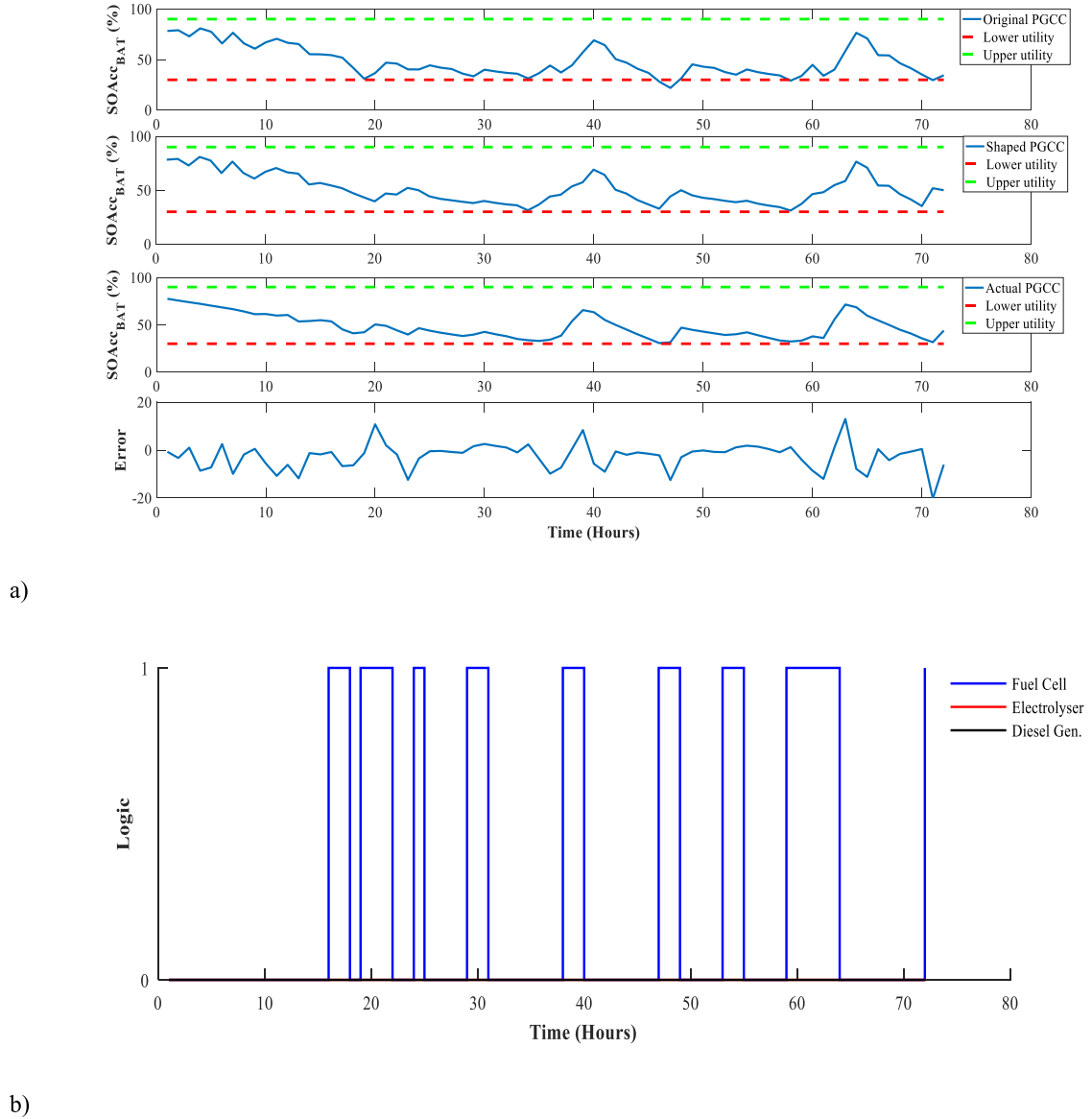


Fig. 10. a) Adaptive Power PoPA, b) State error correction and c) Converter Logic.





**Fig. 11.** (a) The estimated and real Battery SOAcc response with the Kalman Adaptive PoPA for 72 h under Gaussian uncertainty; (b) converter logic.

framework guarantees optimal operation, as long as the conditions of optimal action selection and learning rate decay are satisfied. Figs. 7 and 8, illustrates the RL + Adaptive PoPA architecture and algorithm respectively. Furthermore, the pseudo codes for the proposed algorithms are presented in Appendix I.

## 6. Results and discussion

The three new methods are evaluated against the DA-PoPA in a short (three days (72 h)) and long-term (one year (8760 h)) deployment in a stand-alone HESS. The initial conditions for the  $SOAcc_{BAT}^n$  is such that  $l \in \{BAT, HT \text{ and } WT\}$  corresponds to 70%, 80% and 30% respectively. The HESS parameters used as case study are derived from an existing real system [9] as shown in Table 1. Also, real load demand profiles for a typical residential home and solar irradiance data pertaining to Newcastle, United Kingdom, are sourced from ELEXON [79] and NREL [80] respectively.

The performance main indices (30)–(32) used in evaluating the

EM approaches are with respect to the total number of times the  $S_{Lo}^l$  (30%) and  $S_{Up}^l$  (90%) Pinch limits are violated and the DSL activated, as follows [42];

$$\text{Sum of Deficit} = \sum_{k=1}^{N=8760} \begin{cases} 1 & S_{Lo}^l > SOAcc_{BAT}^n(k) \\ 0 & \text{otherwise} \end{cases} \quad (30)$$

$$\text{Sum Of Surplus} = \sum_{k=1}^{N=8760} \begin{cases} 1 & S_{Up}^l > SOAcc_{BAT}^n(k) \\ 0 & \text{otherwise} \end{cases} \quad (31)$$

$$\text{Sum Of DSL activation} = \sum_{k=1}^{N=8760} \begin{cases} 1 & 20\% > SOAcc_{BAT}^n(k) \\ 0 & \text{otherwise} \end{cases} \quad (32)$$

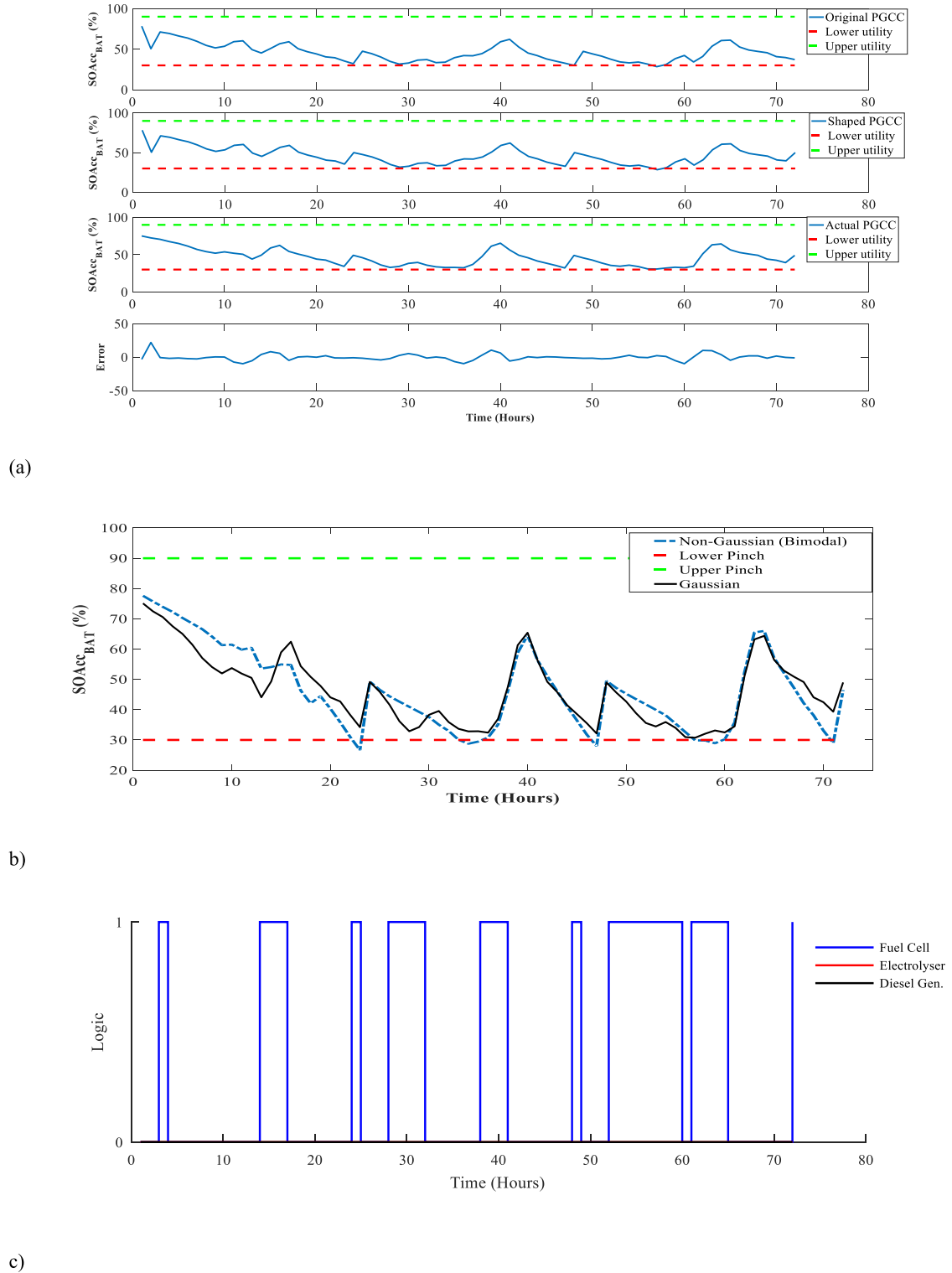


**Fig. 12.** a) The estimated and real Battery SOAcc response with the Kalman Adaptive PoPA for 72 h under Non-Gaussian (Bimodal) uncertainty, b) Comparison of the real SOAcc response under both Gaussian and Non-Gaussian uncertainty, and c) converter logic under non-Gaussian uncertainty.

## 6.1. Short-term operation

### 6.1.1. Day – ahead power pinch analysis

As illustrated in Fig. 9(a), the original PGCC show the  $SOAcc_{BAT}^m$  would dip successively below the  $S_{LO}$  due to impending energy deficit within the first 72 h, if electricity is not outsourced in

advance. Thus, the PGCC is shaped accordingly by activating the FC four times as shown in Fig. 9 (b). However, the PGCC continuously violated  $S_{LO}$  14 time instances which led to the activation of the DSL twice due to uncertainty indicated by the error plot as shown in Fig. 9a, regardless of hydrogen availability.

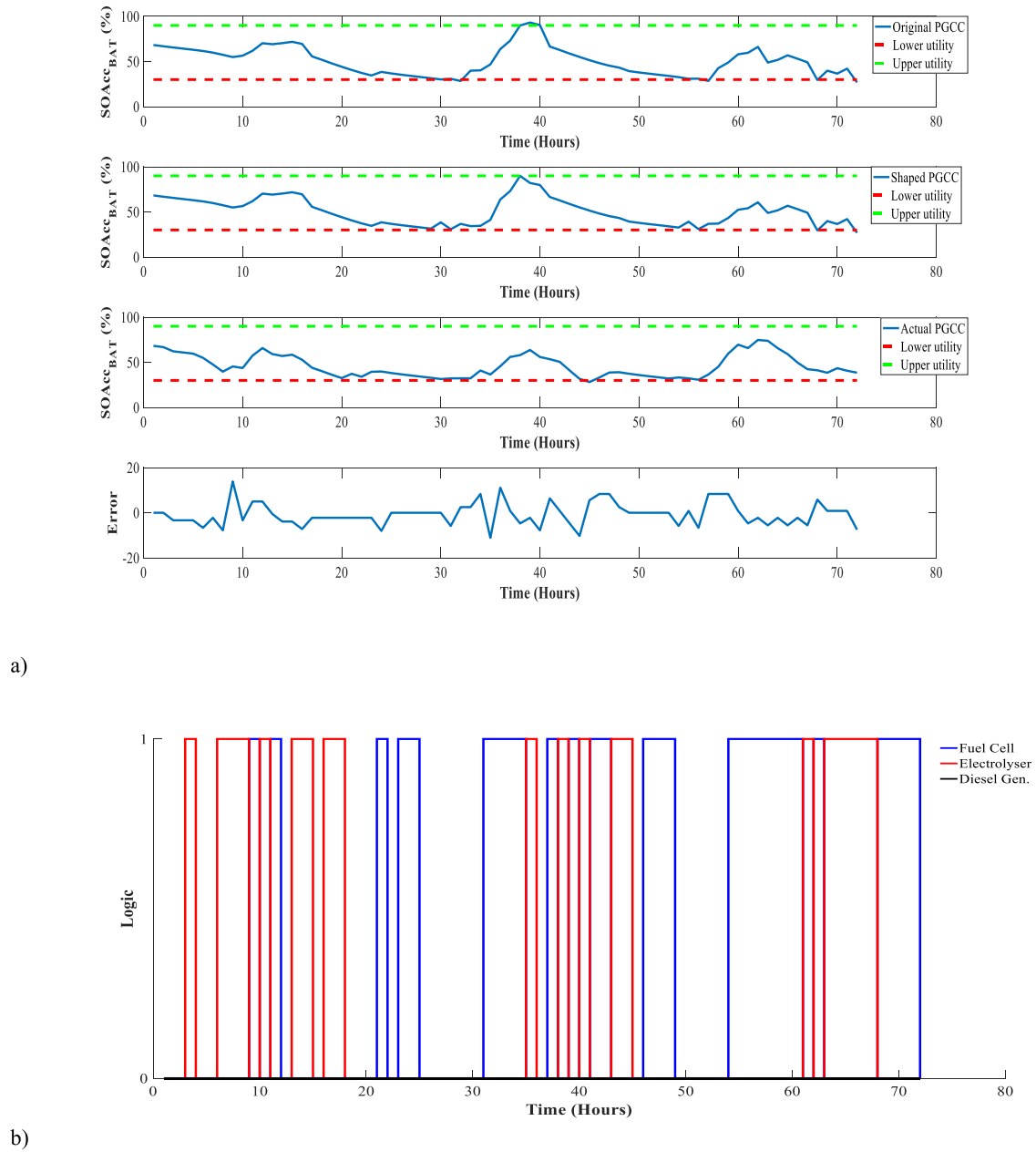


**Fig. 13.** (a) Shows the performance of the RL + Adaptive Pinch strategy for 72 h; (b) converter logic.

**Table 2**

Summary of the performance indices for 72 h.

	Non-Gaussian Uncertainty				Gaussian Uncertainty			
	DA-PoPA	Adaptive PoPA	Kalman + Adaptive PoPA	RL + Adaptive PoPA	DA-PoPA	Adaptive PoPA	Kalman + Adaptive PoPA	RL + Adaptive PoPA
Lower Pinch violation	14	7	7	1	13	3	0	0
Upper Pinch violation	0	0	0	0	0	0	0	0
DSL Activation	2	0	0	0	4	0	0	0

### 6.1.2. Adaptive power pinch analysis energy management strategy for uncertainty

The energy deficit and consequent forecast error deviation exhibited by the DA-PoPA was reduced by the dynamic shaping of the PGCC within a receding control horizon as shown in Fig. 10a. Fig. 10b illustrates the state error correction at the inception of the 11:00 Hr after  $\Delta H$  became greater than 5% at 10:00 h. However, the  $SOAcc_{BAT}^n$  dipped at the 33rd, 34th, 47th, 57th, 58th, 70th, and 71st h, without activating the DSL. Furthermore, despite dispatching the FC six times, as shown in Fig. 10c after the occurrence of the unforeseen dip, a further violation of  $S_{LO}$  re-occurred. This was because the MOES delivered by the FC was less than required, due to deficit energy target variability. The successive dips underscore the need for a preventive approach since the reactive approach only responds after the forecast error has occurred.

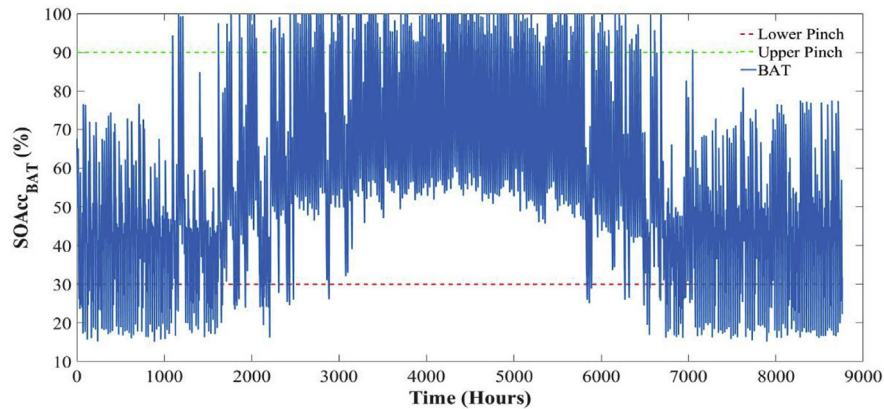
### 6.1.3. Kalman filter adaptive PoPA

The Kalman + Adaptive approach results in the PGCC violating  $S_{LO}$  7 times at time 49:00–56:00 h and at time 64:00–70:00 h, as shown in Fig. 11a. Additionally, the FC was activated 20 times in response to uncertainty with the DSL never activated as shown in Fig. 11 (b). The Kalman + Adaptive PGCC closely matched the actual state of the plant as shown in Fig. 11a, with the uncertainty adequately propagated within the first 48 h, hence, the performance was better than using the Adaptive PoPA alone. However, the uncertainty (previously unknown until now, but expected to be a normal Gaussian distribution) was essentially non-Gaussian (bimodal). Thus, further investigation as illustrated in Fig. 12a and (b) shows that the Kalman + Adaptive PoPA performs better as the variance of forecast error is reduced when the uncertainty is normally distributed. Fig. 12b shows the converter logic. Hence, a more sophisticated approach when the uncertainty is unknown should suffice.

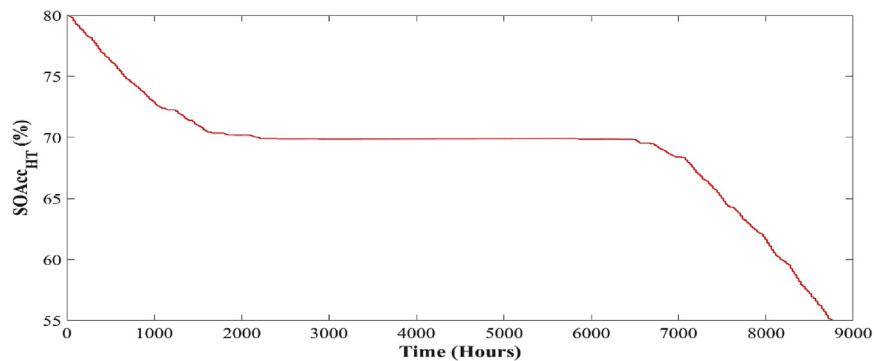
**Table 3**

Performance metrics characterizing the proposed Pinch methods for one year (8760 h) with HT Volume of 15m<sup>3</sup>.

	Day – Ahead PoPA	Adaptive PoPA	Kalman + Adaptive PoPA	RL + Adaptive PoPA
Lower Pinch violation ( $SOAcc_{BAT}^n < 30\%$ )	804	271	64	51
Upper Pinch violation ( $SOAcc_{BAT}^n > 90\%$ )	756	303	265	226
FC start-stop (cycles/year)	296	577	1837	3802
EL start-stop (cycles/year)	262	654	931	3503
DSL start-stop (cycles/year)	229	1	0	0
PV start-stop (cycles/year)	8004	8457	8495	8534



(a)



(b)

**Fig. 14.** (a) The response of the BAT and (b) HT with the DA-PoPA.



#### 6.1.4. RL + Adaptive PoPA

The RL + Adaptive PoPA had only one violation of  $S_{LO}$ , which occurred at the 45th h as shown in Fig. 13a. Also, the DSL was never activated. However, the FC and EL were activated 28 and 20 times respectively in a bid to track the Adaptive PoPA's PGCC as shown in Fig. 13b.

The violation of  $S_{LO}$  as indicated in Table 2, evidently showed Kalman Adaptive PoPA had the most significant improvement from 7 to 0  $S_{LO}$  violations and none for the  $S_{UP}$  under Gaussian uncertainty and non-Gaussian case respectively. The RL Adaptive had no limit violations under the Gaussian uncertainty. While the Adaptive PoPA had an improvement when the uncertainty was Gaussian, there was negligible in the DA-PoPA's performance.

#### 6.2. Long-term operation

The proposed methods are evaluated against the DA-PoPA over a period of 8760 h and the results are shown in Table 3. From Table 3, the DA PoPA method had the worst performance indices as regards excessive charging of BAT ( $SOAcc_{BAT}^n > 90\%$ ) and over-discharging ( $SOAcc_{BAT}^n < 30\%$ ) and consequently fossil fuel utilisation due to the DSL activation, despite a decently sized HT of 15 m<sup>3</sup> (initialised with  $SOAcc_{HT}^n$  at 100%). The lower limit ( $SOAcc_{BAT}^n < 30\%$ ) of the BAT was violated 804 times and accordingly the DSL was activated 229 times. Also, the upper pinch limit ( $SOAcc_{BAT}^n > 90\%$ ) of the BAT was violated 756 times.

Thus, benchmarked against the performance of the DA, the

Adaptive, Kalman + Adaptive and RL + Adaptive PoPA methods led to a reduction in  $S_{LO}$  violation by 66%, 92% and 94%, as well as a decrease in the upper limit violation by 60%, 65% and 70%, respectively. Additionally, the DSL was activated only once with the Adaptive PoPA and was never activated with the Kalman, and RL + Adaptive PoPA. Consequently, a reduction in fossil fuel emission by 99.59%, 100% and 100% was achieved with the Adaptive, Kalman, RL + Adaptive PoPA EMS respectively. Furthermore, the reduction in upper limit violation by the Adaptive, Kalman and RL + Adaptive PoPA methods led to an increase in PV penetration by 6%, 6% and 7% respectively, due to the decreased violation of the PV (ON/OFF) protection constraint.

The RL + Adaptive method had the best performance with the least violations of  $S_{LO}$  and  $S_{UP}$ . However, to counteract the uncertainty, the learning agent increased activation of the FC and EL in the control horizon by 642% and 425% respectively, compared to the dictate of the Adaptive PoPA in the predictive horizon.

Also, the activation of the FC and EL with the Adaptive PoPA was seen to have increased by 95% and 150% and similarly for the Kalman + Adaptive PoPA, it was 520% and 255% respectively, compared to the DA-PoPA.

The available hydrogen in HT at 8760 h is as follows: 55% (DA-PoPA), 45% (Adaptive), 44% (RL + Adaptive) and 19% (Kalman + Adaptive). The  $SOAcc_{HT}^n$  and  $SOAcc_{BAT}^n$  are shown in Figs. 14–17. The Kalman + Adaptive PoPA had the most usage of the hydrogen energy carrier, with the DA-PoPA having the least utilisation.

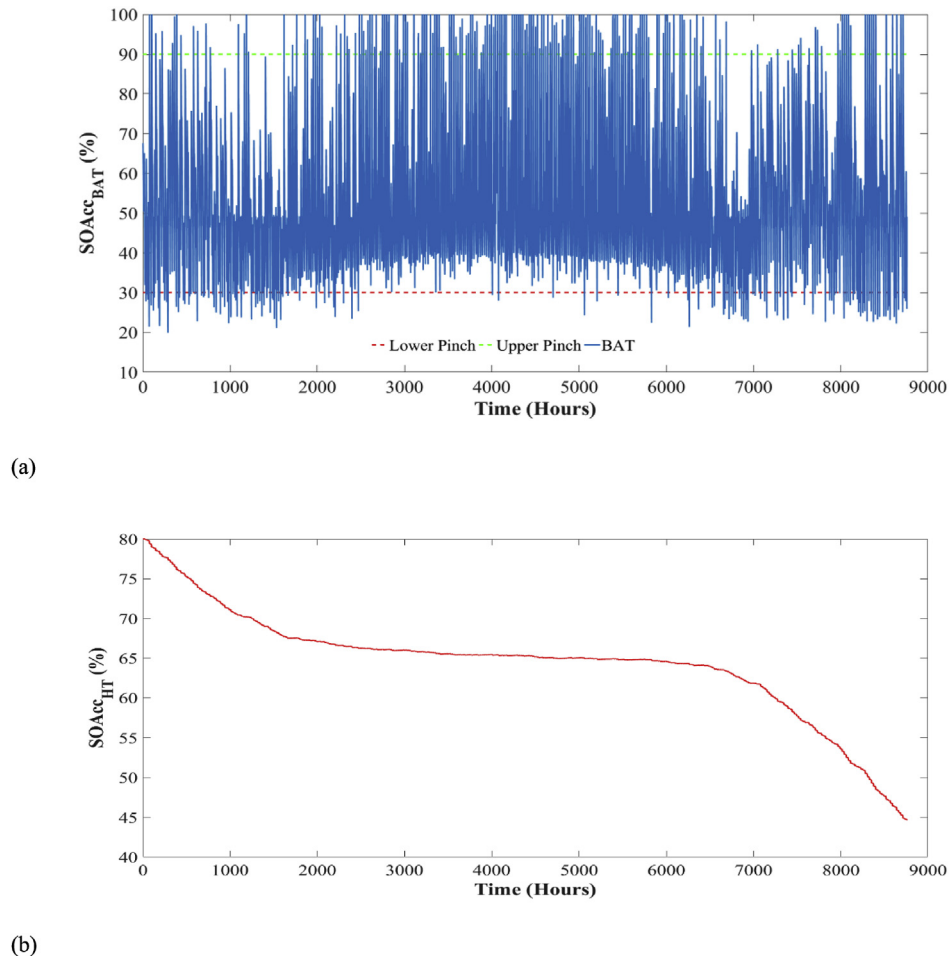
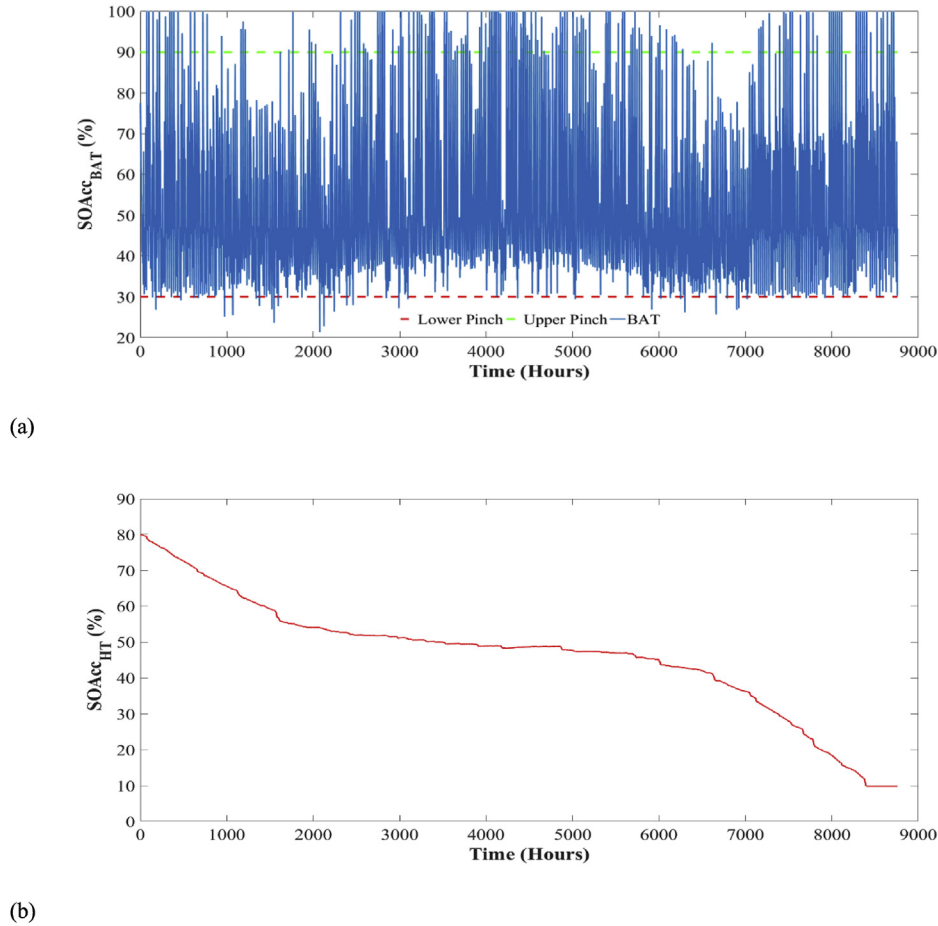


Fig. 15. (a) The response of the BAT and (b) HT with the Adaptive PoPA method.



**Fig. 16.** (a) The response of the BAT and (b) HT response with Kalman + Adaptive PoPA.

### 6.3. Sensitivity analysis of HT size with the PoPA schemes

As shown in Fig. 18, a sensitivity analysis was carried out to investigate the impact of hydrogen uncertainty by varying the HT capacity between 10, 5, and 1 m<sup>3</sup> with the EMS's. The RL + Adaptive PoPA scheme with HT at 10 m<sup>3</sup> had the fewest  $S_{LO}$  and  $S_{UP}$  violations of 68 and 256 times respectively, with the DSL never activated. The Kalman Adaptive PoPA had an  $S_{LO}$  and  $S_{UP}$  violation of 264 and 87 times. The DA-PoPA  $S_{LO}$  and  $S_{UP}$  violations were 756 and 804 times, and the adaptive PoPA violations were 303 and 271. However, the Kalman Adaptive PoPA activated the DSL at 15 instances in response to 87 lower limit violations, compared to the Adaptive PoPA which activated the DSL only once. Decreasing the HT capacity to 5 m<sup>3</sup> and 1 m<sup>3</sup>, the RL + Adaptive PoPA lower limit was violated 1553 and 2616 times respectively, which consequently lead to the activation of the DSL 440 and 782 times.

When considering upper limit violations for different HT sizes, the RL + Adaptive PoPA had the best upper limit violation for an HT of 10 m<sup>3</sup> and 5 m<sup>3</sup>, and the second-best upper limit violation with an HT of 1 m<sup>3</sup>.

The RL + Adaptive PoPA had the least DSL activation overall for HT sizes of 5 m<sup>3</sup> and 1 m<sup>3</sup>, which consequently implies that despite the  $S_{LO}$  violation of 1203 and 2616 times in that order were only better than the Kalman Adaptive PoPA's 1553 and 3468 times respectively. Additionally, as seen in Fig. 17, the preventive methods were more effective when the hydrogen is adequately available (i.e. HT > 5 m<sup>3</sup>) (see Figure A1 in the appendix).

The DA-PoPA violation of the upper limit remained almost

unchanged despite the HT size variation. This clearly indicates the weakness of the DA-PoPA to uncertainty, in event of an unanticipated excess or deficit energy not considered during the daily energy target planning.

## 7. Conclusion

The Adaptive, Kalman + Adaptive and RL + Adaptive PoPA methods have been proposed to counteract uncertainty caused by PV and load profile variation which may impact the reliability of the HESS. These methods were compared against the existing DA-PoPA strategy using real-world data. The Adaptive PoPA had a better performance than the DA-PoPA, as a result of the inclusion of a feedback loop which minimised the effect of forecast deviations. However, the method offered a reactive strategy whose correction mechanism relied on the occurrence of the forecast error. Furthermore, the Adaptive PoPA incorporated a receding horizon without uncertainty propagation. The Kalman + Adaptive PoPA had a better performance than the adaptive PoPA. However, the formulation of the estimator relies on the assumption of a normally distributed uncertainty which was not the case. The RL + Adaptive method, which incorporates a learning agent illustrated for short and long-term operation, was shown to maximise the expected reward by acting optimally to meet the identified pinch targets. The RL + Adaptive had the best response across all performance indices;  $S_{LO}$  and  $S_{UP}$  limits violation as well as reduced diesel carbon footprint when the HT was sized at 10 m<sup>3</sup>. However, even though the RL + Adaptive PoPA method offers the best results with respect

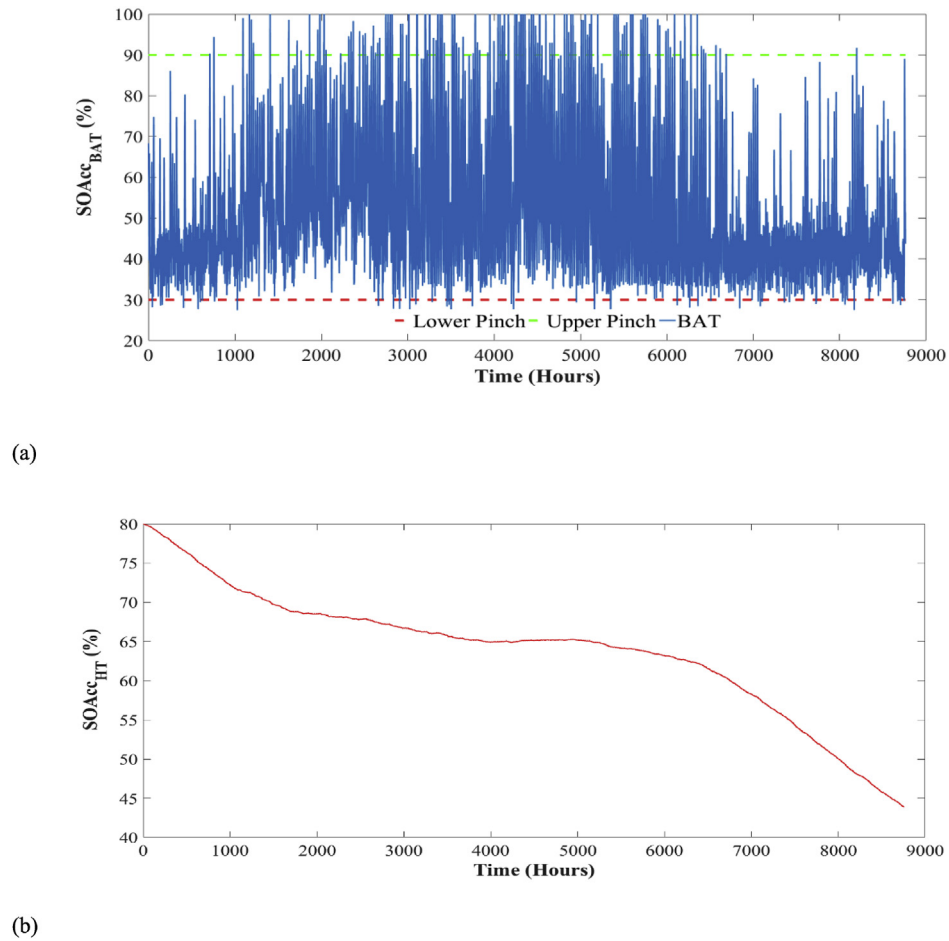


**Fig. 17.** (a) The response of the BAT and (b) HT response using RL + Adaptive Pinch Analysis.

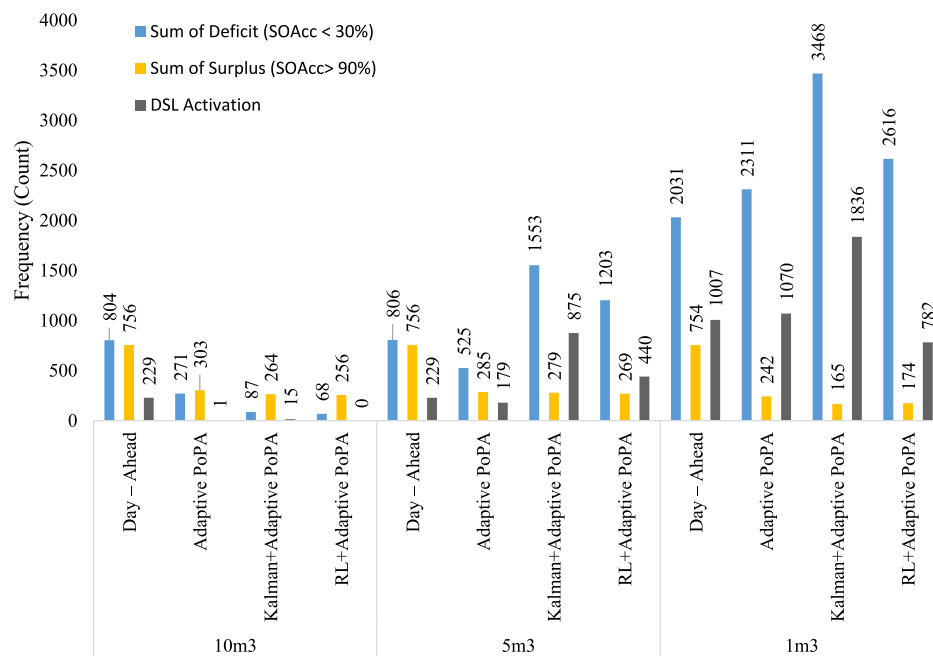


**Fig. 18.** Sensitivity analysis of the PoPA Energy Management Schemes with 10, 5 and 1 m<sup>3</sup> HT capacity.

to an avoided violation of operating limits on the storage devices this excellent performance comes at the cost of increased complexity. Therefore, the method used will be dependent on the application. For example, if there is a high confidence in the load/weather forecast then the DA PoPA method can be used, but if there is some error in the forecast, then the first Adaptive PoPA method, which does not require heavy processing power but is less accurate, should be used. However, if the difference between the real and the forecasted load/weather profile is significant and the uncertainty has specific statistical properties, then the right choice should be the use of the Adaptive PoPA with Kalman filter. Finally, if the error is large with no information about the type of uncertainty, then the RL + Adaptive PoPA should be the choice.

## Acknowledgement

B.E. Nyong-Bassey would like to appreciate the Petroleum Technology Development Fund Nigeria (PTDF/ED/OSS/PHD/SLA/818/16) for their funding and support towards the research.

## Appendix A. Supplementary data

Supplementary data to this article can be found online at <https://doi.org/10.1016/j.energy.2019.116622>.

## References

- [1] Qiao L. A summary of optimal methods for the planning of stand-alone microgrid system. *Energy Power Eng* 2013;5(04):992.
- [2] June Muljadi E, Wang C, Nehrir MH. Parallel operation of wind turbine, fuel cell, and diesel generation sources. In: *Power engineering society general meeting*. IEEE; 2004. p. 1927–32 [IEEE].
- [3] Dorji T, Urmee T, Jennings P. Options for off-grid electrification in the kingdom of Bhutan. *Renew Energy* 2012;45:51–8.
- [4] Kellogg WD, Nehrir MH, Venkataramanan G, Gerez V. Generation unit sizing and cost analysis for stand-alone wind, photovoltaic, and hybrid wind/PV systems. *IEEE Trans Energy Convers* 1998;13(1):70–5.
- [5] Giaouris D, Papadopoulos AI, Voutetakis S, Papadopoulos S, Seferlis P. A power grand composite curves approach for analysis and adaptive operation of renewable energy smart grids. *Clean Technol Environ Policy* 2015;17(5):1171–93.
- [6] Bocklisch T. Hybrid energy storage systems for renewable energy applications. *Energy Procedia* 2015;73:103–11.
- [7] Giaouris D, Papadopoulos AI, Ziogou C, Ipsakis D, Voutetakis S, Papadopoulos S, Seferlis P, Stergiopoulos F, Elmasides C. Performance investigation of a hybrid renewable power generation and storage system using systemic power management models. *Energy* 2013;61:621–35.
- [8] <http://www.systems-sunlight.com/>, [Accessed 1st Nov 2017].
- [9] Ipsakis D, Voutetakis S, Seferlis P, Stergiopoulos F, Elmasides C. Power management strategies for a stand-alone power system using renewable energy sources and hydrogen storage. *Int J Hydrogen Energy* 2009;34(16):7081–95.
- [10] Mahmood H, Michaelson D, Jiang J. A power management strategy for PV/battery hybrid systems in islanded microgrids. *IEEE J Emerg Selected Topics Power Electronics* 2014;2(4):870–82.
- [11] Zhao H, Wu Q, Hu S, Xu H, Rasmussen CN. Review of energy storage system for wind power integration support. *Appl Energy* 2015;137:545–53.
- [12] Fragiaco P, De Lorenzo G, Corigliano O. Performance analysis of an intermediate temperature solid oxide electrolyzer test bench under a CO<sub>2</sub>-H<sub>2</sub>O feed stream. *Energies* 2018;11(9):2276.
- [13] Mougin J, Mansuy A, Chatroux A, Gousseau G, Petitjean M, Reytier M, Mauvy F. Enhanced performance and durability of a high temperature steam electrolysis stack. *Fuel Cells* 2013;13(4):623–30.
- [14] Jiao K, He P, Du Q, Yin Y. Three-dimensional multiphase modeling of alkaline anion exchange membrane fuel cell. *Int J Hydrogen Energy* 2014;39(11):5981–95.
- [15] Jiao K, Huo S, Zu M, Jiao D, Chen J, Du Q. An analytical model for hydrogen alkaline anion exchange membrane fuel cell. *Int J Hydrogen Energy* 2015;40(8):3300–12.
- [16] Olatomiwa L, Mekhilef S, Ismail MS, Moghaviemi M. Energy management strategies in hybrid renewable energy systems: a review. *Renew Sustain Energy Rev* 2016;62:821–35.
- [17] Wiecek M, Lewandowski M. A mathematical representation of an energy management strategy for hybrid energy storage system in electric vehicle and real time optimization using a genetic algorithm. *Appl Energy* 2017;192:222–33.
- [18] Wang S, Tang Y, Shi J, Gong K, Liu Y, Ren L, Li J. Design and advanced control strategies of a hybrid energy storage system for the grid integration of wind power generations. *IET Renew Power Gener* 2014;9(2):89–98.
- [19] Herath A, Kodituwakku S, Dasanayake D, Binduhewa P, Ekanayake J, Samarakoon K. Comparison of optimization-and rule-based EMS for domestic PV-battery installation with time-varying local SoC limits. *J Electric Comp Eng* 2019;2019.
- [20] De Souza BP, Zeni VS, Sica ET, Pica CQ, Hernandez MV. Fuzzy logic energy management system in islanded hybrid energy generation microgrid. In: *2018 IEEE Canadian conference on electrical & computer engineering (CCECE)*. IEEE; 2018. p. 1–5 [May].
- [21] Li X, Xu L, Hua J, Lin X, Li J, Ouyang M. Power management strategy for vehicular-applied hybrid fuel cell/battery power system. *J Power Sources* 2009;191(2):542–9.
- [22] Yu Z, Zinger D, Bose A. An innovative optimal power allocation strategy for fuel cell, battery and supercapacitor hybrid electric vehicle. *J Power Sources* 2011;196(4):2351–9.
- [23] De Lorenzo G, Andaloro L, Sergi F, Napoli G, Ferraro M, Antonucci V. Numerical simulation model for the preliminary design of hybrid electric city bus power train with polymer electrolyte fuel cell. *Int J Hydrogen Energy* 2014;39(24):12934–47.
- [24] Du J, Zhang X, Wang T, Song Z, Yang X, Wang H, Wu X. Battery degradation minimization oriented energy management strategy for plug-in hybrid electric bus with multi-energy storage system. *Energy* 2018;165:153–63.
- [25] Aktas A, Erhan K, Özdemir S, Özdemir E. Dynamic energy management for photovoltaic power system including hybrid energy storage in smart grid applications. *Energy* 2018;162:72–82.
- [26] Zhao LUO, Wei GU, Zhi WU, Zhihe WANG, Yiyuan TANG. A robust optimization method for energy management of CCHP microgrid. *J Modern Power Syst Clean Energy* 2018;6(1):132–44.
- [27] Zhang Y, Fu L, Zhu W, Bao X, Liu C. Robust model predictive control for optimal energy management of island microgrids with uncertainties. *Energy* 2018;164:1229–41.
- [28] Buhmann JM, Gronskiy AY, Mihalák M, Pröger T, Šrámek R, Widmayer P. Robust optimization in the presence of uncertainty: a generic approach. *J Comput Syst Sci* 2018;94:135–66.
- [29] Hadayeghparast S, Farsangi AS, Shayanfar H. Day-ahead stochastic multi-objective economic/emission operational scheduling of a large scale virtual power plant. *Energy* 2019;127.
- [30] Hu MC, Lu SY, Chen YH. Stochastic programming and market equilibrium analysis of microgrids energy management systems. *Energy* 2016;113:662–70.
- [31] Tabar VS, Jirdehi MA, Hemmati R. Energy management in microgrid based on the multi objective stochastic programming incorporating portable renewable energy resource as demand response option. *Energy* 2017;118:827–39.
- [32] Hu MC, Lu SY, Chen YH. Stochastic programming and market equilibrium analysis of microgrids energy management systems. *Energy* 2016;113:662–70.
- [33] Cai M, Huang G, Chen J, Li Y, Fan Y. A generalized fuzzy chance-constrained energy systems planning model for Guangzhou, China. *Energy* 2018;165:191–204.
- [34] Li Y, Yang Z, Li G, Zhao D, Tian W. Optimal scheduling of an isolated microgrid with battery storage considering load and renewable generation uncertainties. *IEEE Trans Ind Electron* 2019;66(2):1565–75.
- [35] Huang Y, Wang L, Guo W, Kang Q, Wu Q. Chance constrained optimization in a home energy management system. *IEEE Trans Smart Grid* 2018;9(1):252–60.
- [36] Bruni G, Cordiner S, Mulone V, Sinisi V, Spagnolo F. Energy management in a domestic microgrid by means of model predictive controllers. *Energy* 2016;108:119–31.
- [37] Xiang C, Ding F, Wang W, He W, Qi Y. MPC-based energy management with adaptive Markov-chain prediction for a dual-mode hybrid electric vehicle. *Sci China Technol Sci* 2017;60(5):737–48.
- [38] Li X, Han L, Liu H, Wang W, Xiang C. Real-time optimal energy management strategy for a dual-mode power-split hybrid electric vehicle based on an explicit model predictive control algorithm. *Energy* 2019;127.
- [39] Giaouris D, Papadopoulos AI, Patsios C, Walker S, Ziogou C, Taylor P, Voutetakis S, Papadopoulos S, Seferlis P. A systems approach for management of microgrids considering multiple energy carriers, stochastic loads, forecasting and demand side response. *Appl Energy* 2018;226:546–59.
- [40] Papadopoulos AI, Giannakoudis G, Seferlis P, Voutetakis S. Efficient design under uncertainty of renewable power generation systems using partitioning and regression in the course of optimization. *Ind Eng Chem Res* 2012;51(39):12862–76.
- [41] Bandyopadhyay S. Design and optimization of isolated energy systems through pinch analysis. *Asia Pac J Chem Eng* 2011;6:518–26.
- [42] Alwi SRW, Rozali NEM, Abdul-Manan Z, Klemes JJ. A process integration targeting method for hybrid power systems. *Energy* 2012;44(1):6–10.
- [43] Linnhoff B, Flower JR. Synthesis of heat exchanger networks: I. Systematic generation of energy optimal networks. *AIChE J* 1978;24(4):633–42.
- [44] Smith R. Chemical process: design and integration. John Wiley & Sons; 2005.
- [45] Varbanov PS, Fodor Z, Klemes JJ. Total Site targeting with process specific minimum temperature difference ( $\Delta T_{min}$ ). *Energy* 2012;44(1):20–8.
- [46] Norbu S, Bandyopadhyay S. Power Pinch Analysis for optimal sizing of renewable-based isolated system with uncertainties. *Energy* 2017;135:466–75.
- [47] Rozali NEM, Alwi SRW, Manan ZA, Klemes JJ, Hassan MY. Process integration



- techniques for optimal design of hybrid power systems. *Appl Therm Eng* 2013;61(1):26–35.
- [48] Esfahani IJ, Lee S, Yoo C. Extended-power pinch analysis (EPoPA) for integration of renewable energy systems with battery/hydrogen storages. *Renew Energy* 2015;80:1–14.
- [49] Giaouris D, Papadopoulos AI, Seferlis P, Voutetakis S, Papadopolou S. Power grand composite curves shaping for adaptive energy management of hybrid microgrids. *Renew Energy* 2016;95:433–48.
- [50] Brka A, Al-Abdeli YM, Kothapalli G. Predictive power management strategies for stand-alone hydrogen systems: operational impact. *Int J Hydrogen Energy* 2016;41(16):6685–98.
- [51] Dias LS, Ierapetritou MG. Integration of scheduling and control under uncertainties: review and challenges. *Chem Eng Res Des* 2016;116:98–113.
- [52] Richards A, How J. Robust model predictive control with imperfect information. In: *Proceedings of the 2005. American Control Conference IEEE*; 2005. p. 268–73.
- [53] Bemporad Alberto, Borrelli Francesco, Morari Manfred. Min-max control of constrained uncertain discrete-time linear systems. *IEEE Trans Autom Control* 2003;48(9):1600–6.
- [54] Siswanto J, Prabuwo AS, Abdullah A, Idris B. A linear model based on Kalman filter for improving neural network classification performance. *Expert Syst Appl* 2016;49:112–22.
- [55] Takeda H, Tamura Y, Sato S. Using the ensemble Kalman filter for electricity load forecasting and analysis. *Energy* 2016;104:184–98.
- [56] Al-Hamadi HM, Soliman SA. Short-term electric load forecasting based on Kalman filtering algorithm with moving window weather and load model. *Electr Power Syst Res* 2004;68(1):47–59.
- [57] Sutton RS. Learning to predict by the methods of temporal differences. *Mach Learn* 1988;3(1):9–44.
- [58] Geramifard A, Walsh TJ, Tellex S, Chowdhary G, Roy N, How JP. A tutorial on linear function approximators for dynamic programming and reinforcement learning. *Found Trends® Mach Learn* 2013;6(4):375–451.
- [59] Watkins CJ, Dayan P. Q-learning. *Mach Learn* 1992;8(3–4):279–92.
- [60] ALTUNTAŞ N, Imal E, Emanet N, Öztürk CN. Reinforcement learning-based mobile robot navigation. *Turk J Electr Eng Comput Sci* 2016;24(3):1747–67.
- [61] Zhang Q, Li M, Wang X, Zhang Y. Reinforcement learning in robot path optimization. *JSW* 2012;7(3):657–62.
- [62] Sutton RS. Dyna, an integrated architecture for learning, planning, and reacting. *ACM SIGART Bull* 1991;2(4):160–3.
- [63] Ernst D, Glavic M, Capitanescu F, Wehenkel L. Reinforcement learning versus model predictive control: a comparison on a power system problem. *IEEE Trans Syst Man Cybern Part B (Cybern)* 2009;39(2):517–29.
- [64] Peng K, Morrison C. Model predictive prior reinforcement learning for a heat pump thermostat. In: *IEEE international conference on automatic computing: feedback computing*, vol. 16; July 2016.
- [65] Kuznetsova E, Li YF, Ruiz C, Zio E, Ault G, Bell K. Reinforcement learning for microgrid energy management. *Energy* 2013;59:133–46.
- [66] François-Lavet V, Taralla D, Ernst D, Fonteneau R. Deep reinforcement learning solutions for energy microgrids management. In: *European workshop on reinforcement learning*. EWRL; 2016. 2016.
- [67] Kofinas P, Dounis AI, Vouros GA. Fuzzy Q-Learning for multi-agent decentralized energy management in microgrids. *Appl Energy* 2018;219:53–67.
- [68] Liu T, Wang B, Yang C. Online Markov chain-based energy management for a hybrid tracked vehicle with speedy Q-learning. *Energy* 2018;160:544–55.
- [69] Rocchetta R, Bellani L, Compare M, Zio E, Patelli E. A reinforcement learning framework for optimal operation and maintenance of power grids. *Appl Energy* 2019;241:291–301.
- [70] Xiong R, Cao J, Yu Q. Reinforcement learning-based real-time power management for hybrid energy storage system in the plug-in hybrid electric vehicle. *Appl Energy* 2018;211:538–48.
- [71] Lin X, Wang Y, Bogdan P, Chang N, Pedram M. Reinforcement learning based power management for hybrid electric vehicles. In: *Proceedings of the 2014 IEEE/ACM international conference on computer-aided design*. IEEE Press; 2014. p. 32–8.
- [72] International symposium on. *IEEE*; 2018 May. p. 1–5.
- [73] Nyong-Bassey BE, Giaouris D, Patsios H, Gadoue AI, Papadopolou Seferlis P, Voutetakis S, Papadopoulos S. 'A probabilistic adaptive model predictive power pinch analysis (PoPA) energy management approach to uncertainty'. In: *9th international conference on power electronics, machines and drives (PEMD)*. Journal of engineering. IET; 2018.
- [74] December Tijssma AD, Drugan MM, Wiering MA. Comparing exploration strategies for Q-learning in random stochastic mazes. In: *Computational intelligence (SSCI)*, 2016 IEEE symposium series on. IEEE; 2016. p. 1–8.
- [75] Carden SW. Convergence of a reinforcement learning algorithm in continuous domains (Doctoral dissertation. Clemson University); 2014.
- [76] Campbell JS, Givigi SN, Schwartz HM. Multiple model Q-learning for stochastic asynchronous rewards. *J Intell Robot Syst* 2016;81(3–4):407–22.
- [77] Tokic M September. Adaptive  $\epsilon$ -greedy exploration in reinforcement learning based on value differences. In: *Annual conference on artificial intelligence*. Berlin, Heidelberg: Springer; 2010. p. 203–10.
- [78] Bellman R. Dynamic programming. Courier Corporation; 2013.
- [79] <http://data.ukedc.rl.ac.uk/simplebrowse/edc/efficiency/residential/LoadProfile/data> [Accessed 1st Nov. 2017].
- [80] <http://pvwatts.nrel.gov/pvwatts.php>, [Accessed 1st Nov 2017].